FAKULTA MECHATRONIKY,
INFORMATIKY A MEZIOBOROVÝCH
STUDIÍ TUL

Bakalářská práce

Fabrication and functionalization of graphene-based materials: comparison between experiment and density functional theory calculations

Studijní program: B0719A130001 Nanotechnologie
Autor práce: **Michal Salava**
Vedoucí práce: doc. Ing. Stanislaw Waclawek, Ph.D.
Ústav nových technologií a aplikované informatiky

Konzultant práce: Mgr. Daniele Silvestri, Ph.D.
Ústav pro nanomateriály, pokročilé technologie a inovace

Liberec 2024

FAKULTA MECHATRONIKY,
INFORMATIKY A MEZIOBOROVÝCH
STUDIÍ TUL

Zadání bakalářské práce

Fabrication and functionalization of graphene-based materials: comparison between experiment and density functional theory calculations

Jméno a příjmení:	**Michal Salava**
Osobní číslo:	M21000083
Studijní program:	B0719A130001 Nanotechnologie
Zadávající katedra:	Ústav nových technologií a aplikované informatiky
Akademický rok:	2023/2024

Zásady pro vypracování:

1. Fabrication and functionalization of graphene-based materials (Hummers method, electrochemical method, further modifications of thus obtained graphene-based materials).
2. Characterization of graphene-based materials (FTIR, Raman, etc.).
3. Comparing characterization of graphene-based materials obtained by the experimental methods with density functional theory calculations.

Rozsah grafických prací:	dle potřeby dokumentace
Rozsah pracovní zprávy:	30 – 40 stran
Forma zpracování práce:	tištěná/elektronická
Jazyk práce:	angličtina

Seznam odborné literatury:

[1] PARVEZ, Khaled; Zhong-Shuai WU; Rongjin LI; Xianjie LIU; Robert GRAF et al. Exfoliation of Graphite into Graphene in Aqueous Solutions of Inorganic Salts. online. *Journal of the American Chemical Society*, vol. 136 (2014), no. 16, pp. 6083–6091. Available from: https://doi.org/10.1021/ja5017156

[2] VENKATESHAIAH, Abhilash; Jun Young CHEONG; Christoph HABEL; Stanislaw WACŁAWEK; Tomáš LEDERER et al. Tree Gum–Graphene Oxide Nanocomposite Films as Gas Barriers. online. *ACS Applied Nano Materials*, vol. 3 (2020), no. 1, pp. 633–640. Available from: https://doi.org/10.1021/acsanm.9b02166

[3] HE, Hongkun and Chao GAO. General Approach to Individually Dispersed, Highly Soluble, and Conductive Graphene Nanosheets Functionalized by Nitrene Chemistry. online. *Chemistry of Materials*, vol. 22 (2010), no. 17, pp. 5054–5064. Available from: https://doi.org/10.1021/cm101634k

[4] LAI, Linfei; Luwei CHEN; Da ZHAN; Li SUN; Jinping LIU et al. One-step synthesis of NH2-graphene from in situ graphene-oxide reduction and its improved electrochemical properties. online. *Carbon*, vol. 49 (2011), no. 10, pp. 3250–3257. Available from: https://doi.org/10.1016/j.carbon.2011.03.051

[5] ROHINI, K.; Daniel M. R. SYLVINSON and R. S. SWATHI. Intercalation of HF, H2O, and NH3 Clusters within the Bilayers of Graphene and Graphene Oxide: Predictions from Coronene-Based Model Systems. online. *The Journal of Physical Chemistry A*, vol. 119 (2015), no. 44, pp. 10935–10945. Available from: https://doi.org/10.1021/acs.jpca.5b05702

Vedoucí práce:	doc. Ing. Stanislaw Waclawek, Ph.D. Ústav nových technologií a aplikované informatiky
Konzultant práce:	Mgr. Daniele Silvestri, Ph.D. Ústav pro nanomateriály, pokročilé technologie a inovace
Datum zadání práce:	12. října 2023
Předpokládaný termín odevzdání:	14. května 2024

L.S.

prof. Ing. Zdeněk Plíva, Ph.D.
děkan

prof. Ing. Josef Šedlbauer, Ph.D.
garant studijního programu

V Liberci dne 19. října 2023

Prohlášení

Prohlašuji, že svou bakalářskou práci jsem vypracoval samostatně jako původní dílo s použitím uvedené literatury a na základě konzultací s vedoucím mé bakalářské práce a konzultantem.

Jsem si vědom toho, že na mou bakalářskou práci se plně vztahuje zákon č. 121/2000 Sb., o právu autorském, zejména § 60 – školní dílo.

Beru na vědomí, že Technická univerzita v Liberci nezasahuje do mých autorských práv užitím mé bakalářské práce pro vnitřní potřebu Technické univerzity v Liberci.

Užiji-li bakalářskou práci nebo poskytnu-li licenci k jejímu využití, jsem si vědom povinnosti informovat o této skutečnosti Technickou univerzitu v Liberci; v tomto případě má Technická univerzita v Liberci právo ode mne požadovat úhradu nákladů, které vynaložila na vytvoření díla, až do jejich skutečné výše.

Současně čestně prohlašuji, že text elektronické podoby práce vložený do IS/STAG se shoduje s textem tištěné podoby práce.

Beru na vědomí, že má bakalářská práce bude zveřejněna Technickou univerzitou v Liberci v souladu s § 47b zákona č. 111/1998 Sb., o vysokých školách a o změně a doplnění dalších zákonů (zákon o vysokých školách), ve znění pozdějších předpisů.

Jsem si vědom následků, které podle zákona o vysokých školách mohou vyplývat z porušení tohoto prohlášení.

15. května 2024 Michal Salava

Fabrication and functionalization of graphene-based materials: comparison between experiment and density functional theory calculations

Abstract

Since its discovery in 2004, graphene and its derivatives—collectively known as graphene-based materials (GBM)—have intrigued scientists with their potential to revolutionize various industries. This thesis investigates the synthesis of oxidized graphene-based materials using both the traditional, hazardous Hummers method and a novel, environmentally friendly electrochemical exfoliation technique. The study demonstrates that electrochemical exfoliation may address several significant challenges currently impeding the widespread application of graphene-based materials, including those related to large-scale production and the environmental and temporal costs associated with traditional fabrication methods. In this work, we successfully synthesized graphene-based materials using both methods mentioned above, incorporating a novel chemical agent for the electrochemical exfoliation process. Both sets of materials were then functionalized with ethylenediamine (EDA) and subjected to comprehensive characterization. Spectroscopic techniques such as Fourier Transform Infrared Spectroscopy (FTIR) and Raman Spectroscopy were employed to evaluate and thoroughly compare the outcomes of the two procedures. Furthermore, Scanning electron microscopy (SEM) and Energy-dispersive X-ray spectroscopy (EDS) were used to study the morphology and composition of produced materials.

Additionally, the properties of the synthesized materials were investigated not only experimentally but also through theoretical approaches, including Density Functional Theory (DFT) and semi-empirical method. Given the complex and large-scale structure of graphene-based materials, which encompass thousands of atoms and would require prohibitive computational resources, simplified models using coronene and its derivatives were utilized. These models facilitated the calculations of the spectroscopic properties of graphene-based materials, providing insights that bridge theoretical predictions with experimental observations.

Keywords: Graphene-based materials, graphene oxide, functionalization, DFT

Výroba a funkcionalizace materiálů na bázi grafenu: srovnání experimentu a výpočtů teorie funkcionálu hustoty

Abstrakt

Od jeho objevení v roce 2004 grafen a jeho deriváty—dohromady označován jako materiály na bázi grafenu—zaujali vědce svým potenciálem přivést revoluci do různých odvětvý průmyslu. Tato bakalářská práce zkoumá syntézu oxidovaných materiálů na bázi grafenu za použití tradiční, nebezpečné Hummerovy metody a nové, ekologicky šetrné techniky elektrochemické exfoliace. Studie ukazuje, že elektrochemická exfoliace by mohla vyřešit několik značných problémů, které v současné době brání širokému uplatnění materiálů na bázi grafenu, které souvisí s velkoobjemovou produkcí a enviromentálními a časovými náklady spojenými s tradičními výrobními metodami. V této práci, jsme úspěšně syntetizovali materiály na bázi grafenu pomocí obou výše zmíněných metod, přičemž jsme pro proces elektrochemické exfoliace použily nové chemické činidlo. Oba materiály byly poté funkcializovány ethylendiaminem (EDA) a podrobeny komplexní charakterizaci. Spektroskopické techniky jako infračervená spektroskopie s Fourierovou transformací (FTIR) a Ramanova spektroskopie byly využity k důkladnému vyhodnocení a porovnání obou výsledků. Dále byly ke studiu morfologie a složení vyrobených materiálů použity skenovací elektronová mikroskopie (SEM) a energiově disperzní rentgenová spektrometrie (EDS).

Vlastnosti syntetizovaných materiálů byly studovány nejen experimentálně, ale taté teoreticky, použitím teorie funkcionálu hustoty (DFT) a semiempirické metody. Vzhledem ke složité a rozsáhlé struktuře materiálů na bázi grafenu, která zahrnuje tisíce atomů a vyžadovala by neúnosné výpočetní prostředky, byly využity zjednodušené modely využívající coronene a jeho deriváty. Tyto modely usnadnily výpočty spektroskopických vlastností materiálů na bázi grafenu a poskytly poznatky, které propojují teoretické předpovědi s experimentálním pozorováním.

Klíčová slova: Materiály na bázi grafenu, grafen oxid, funkcionalizace, DFT

Acknowledgements

I would like to greatly thank my thesis supervisor, doc. Ing. Stanisław Wacławek, Ph.D., for his experienced insight and ideas on my thesis topic and for help with correcting the thesis. Further, I would like to thank my consultant Mgr. Daniele Silvestri, Ph.D., for his patience and help with my work in the laboratory. Next, I would like to thank Ing. Martin Stuchlík for FTIR and Raman spectroscopy analysis and Ing. Pavel Kejzlar, Ph.D., for SEM and EDS analysis.

I would like to express my gratitude to my mother for her unwavering support of whatever I choose to pursue. I also want to thank my father for his calm-headed nature, especially in times when I find myself in trouble. I must thank my sister, who has been my best talking buddy and is always there to listen to and understand me better than anybody else.

The authors acknowledge the assistance provided by the Research Infrastructure NanoEnviCz, supported by the Ministry of Education, Youth and Sports of the Czech Republic under Project No. LM2023066. Computational resources were provided by the e-INFRA CZ project (ID:90254), supported by the Ministry of Education, Youth and Sports of the Czech Republic. ChatGPT 4.0 was used to help with corrections of the text and to help with finding references for this work.

Contents

List of figures

List of abbreviations

CNTs	Carbon nanotubes
DFT	Density functional theory
EDA	Ethylenediamine
EDS	Energy-dispersive X-ray spectroscopy
FTIR	Fourier-transform infrared spectroscopy
GBM	Graphene-based materials
GO	Graphene oxide
GO-EDA	GO functionalized by EDA
GrO	Graphene oxide
GrO-EDA	GrO functionalized by ED
HF	Hartree-Fock
KS	Kohn-Sham
SEM	Scanning Electron Microscope

1 Introduction

Carbon, a pivotal element on Earth, is ubiquitously found in an extensive array of derivatives across nearly all organic compounds. It naturally exists predominantly in two allotropes: diamond and graphite. In the diamond allotrope, carbon atoms are organized into a periodic crystalline structure characterized by sp^3 hybridization. Conversely, graphite, another crystalline form of carbon, consists of planar sheets where carbon atoms form a honeycomb lattice through sp^2 hybridization. These individual graphite sheets are primarily interconnected by van der Waals forces, a weak noncovalent interaction [1].

1.1 Carbon allotropes

With the advancement of characterization techniques and the capability to analyse materials at the nanoscale, the turn of the millennium witnessed the discovery of three new carbon allotropes: fullerenes, carbon nanotubes, and graphene. These materials are characterized by the significant feature that at least one of their dimensions measures in the nanometer scale [2]. In 1985, fullerenes were first discovered through the chemical vapour deposition of carbon in a helium atmosphere by Curl, Kroto and Smalley. These are spherical carbon compounds, comprising atoms arranged in hexagonal and pentagonal cycles bonded through sp2 hybridization to form a sphere, containing a precise number of carbon atoms (e.g., C60, C70) [3]. Subsequently, in 1991, Iijima identified and described carbon nanotubes (CNTs), another allotrope where carbon atoms bonded in a hexagonal lattice (sheets of graphene) are "rolled " to form a hollow cylindrical shape [4]. Finally, in 2004, after extensive scientific investigation, graphene—a single layer of graphite—was isolated and thoroughly characterized by Geim and Novoselov. This groundbreaking discovery happened during their Friday night experiments, where they isolated a thin layer (few atoms) from graphite by scotch tape. This material, derived from graphite, demonstrated exceptional properties and swiftly garnered significant interest for scientific research [5].

These seminal discoveries played a vital role in invoking the emergence of nanotechnology, a scientific discipline dedicated to the study of materials with characteristic dimensions at the nanometer scale. By definition, nanomaterials are those that possess at least one dimension measuring less than 100 nm. Depending on the number of dimensions in which a material does not exhibit nanoscale properties, they can be classified into 0D (zero-dimensional), 1D (one-dimensional), and 2D (two-dimensional) nanomaterials. Fullerenes, CNTs, and graphene

serve as quintessential examples of 0D, 1D, and 2D nanomaterials, respectively [6]. The structures of all aforementioned carbon allotropes, both natural and synthetic, are illustrated in Figure 1.

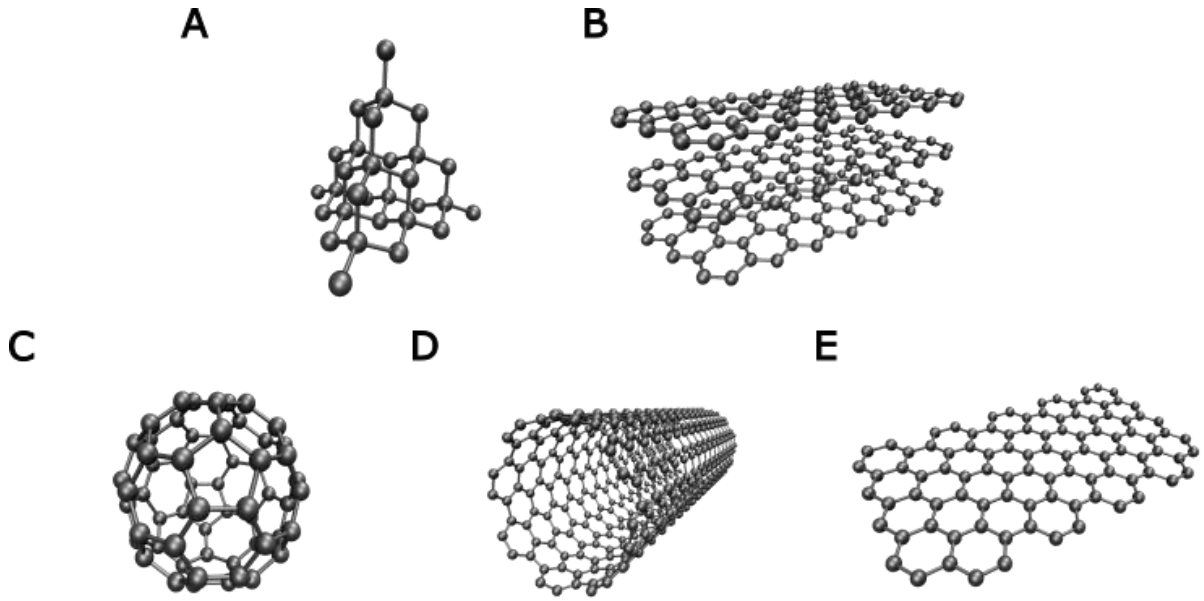

Figure 1: Structures of carbon allotropes: **A** diamond lattice, **B** graphite layers, **C** fullerene C60, **D** carbon nanotube and **E** graphene (one layer of graphite).

1.2 Graphene

Graphene, along with other graphene-based materials (GBM), has rapidly emerged as one of the most extensively researched novel materials across a broad spectrum of scientific fields due to its unique structure and extraordinary properties. This intriguing material has been subject to in-depth study over the years. Graphene comprises a single layer of sp^2 hybridized carbon atoms—similar to graphite and CNTs—arranged in a honeycomb lattice with a bond length of 1.42 Å [7]. Its distinction lies in being a mere single layer of carbon atoms, which bestows upon it an immense surface-to-volume ratio, a characteristic shared with many nanomaterials, thus rendering it an exceptional candidate for sensing and adsorption applications among others [8–10]. Moreover, the sp^2 hybridization facilitates each carbon atom in contributing its π electrons to a delocalized electron system above and below the graphene plane, endowing graphene with remarkable conductive properties. These electrical properties, coupled with its significant surface area, render graphene an ideal material for use in electronic devices

and fuel cells [11]. Furthermore, the strong covalent bonding in graphene's periodic structure imparts remarkable physical properties, including toughness and flexibility. This makes graphene a valuable additive for enhancing the mechanical properties of construction materials and for application in flexible or wearable technology [12, 13]. Despite the global scientific community's extensive efforts to explore graphene (as illustrated in Figure 2), challenges remain that hinder the full exploitation of its potential. Nonetheless, due to its myriad of compelling characteristics, graphene continues to be regarded by many as a material with the potential to revolutionize numerous industries, though barriers to its complete utilization persist [14].

Graphene, as noted previously, boasts an array of remarkable physical properties. However, its structural configuration, which underpins these attributes, also introduces certain limitations, particularly in terms of its chemical properties. The lattice of graphene is characterized by strong σ-bonds between carbon atoms, rendering it a nonpolar compound, and its tendency to agglomerate due to π-π stacking of graphene sheets. Consequently, graphene demonstrates hydrophobic behaviour, complicating the creation of stable dispersions in polar solvents such as water. The practicable solvents for graphene are primarily non-polar, yet these are often toxic and volatile, significantly narrowing the scope of graphene's applications and posing challenges for its industrial-scale utilization [15]. Moreover, despite graphene's physical robustness—even as a monolayer of atoms—it exhibits considerable chemical resistance to a multitude of reactions. This resistance complicates efforts to chemically modify and tailor graphene for specific applications, presenting an additional layer of difficulty in exploiting its full potential [16].

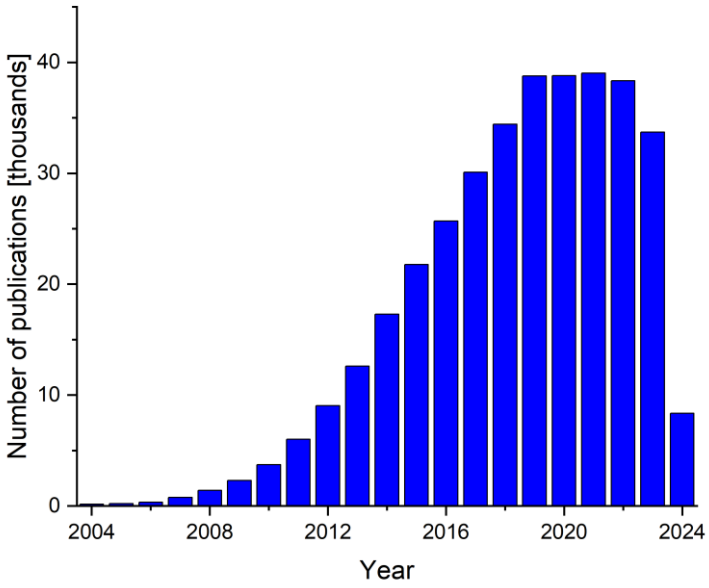

Figure 2: Number of publications per year for keyword “graphene”. Data were taken from database of ISN Web of Science (data from May 2024).

1.3 Graphene and graphite oxide

In order to address the aforementioned challenges associated with GBM, functionalizations are essential. Historically, the Hummers method has been the most prevalent technique for the fabrication of functionalized GBM [graphite oxide (GrO)] [17]. This method, extensively researched and optimized over time, now employs a modified protocol that reduces the use of hazardous chemicals. It fundamentally relies on the application of strong acids and oxidizing agents over several days to incorporate oxygen-containing functional groups—such as hydroxyl, epoxy and carboxyl—into the structure of GBM [18]. The bonds of these functional groups exhibit different properties in terms of length and energy, in contrast to the uniform bonding system of graphite, which enables their detection through spectroscopic methods such as FTIR and Raman spectroscopy. However, the requirement for a significant volume of hazardous chemicals renders the process costly, environmentally detrimental, and challenging to scale for industrial production. Consequently, there is an urgent demand for more sustainable and scalable methods to produce oxidized GBM. In response to this need, recent years have witnessed the development of novel, environmentally friendly approaches, notably the electrochemical method [19, 20]. This technique facilitates the production of graphene oxide (GO)

from graphite sheets through electrochemical exfoliation. In this process, a graphite sheet, serving as an anode, is positioned within a reaction chamber opposite a cathode, typically made of platinum or titanium [21]. The chamber is filled with an electrolyte—commonly a water solution of inorganic salts—which acts as the oxidizing agent. This innovative method represents a significant stride towards greener production processes for GBM, leveraging electrochemical principles to minimize environmental impact and potentially ease the transition to industrial-scale applications [22].

The oxidation process introduces oxygen functional groups onto the planar surfaces of graphene, fundamentally altering its electronic and chemical properties [23]. The high electronegativity of oxygen disrupts the previously uniform electron distribution within the graphene planes, drawing electrons towards these oxygen groups and significantly increasing the material's overall polarity. This increased polarity of GO facilitates the formation of stable dispersions in water, thereby broadening its applicability in aqueous environments [24]. Furthermore, oxidation compromises the sp^2 bonding network of carbon atoms in graphene, disrupting the π-electron cloud that extends above and below the GO plane. This disruption renders GO non-conductive, a property markedly distinct from pristine graphene. However, the conductivity of GO can be partially reinstated through the reduction of oxygen functional groups. Among various reduction methods, the simplest and most commonly employed involves physical reduction at elevated temperatures and pressures [25, 26]. This process of oxidation followed by reduction provides a foundational approach for the functionalization of GBM, enabling the fine-tuning of their properties for specific applications. The structural transformations from graphite to GO, and subsequently to reduced graphene oxide (rGO), are illustrated in Figure 3. Models for graphene structures were created utilizing python script made by Muaru et al [27].

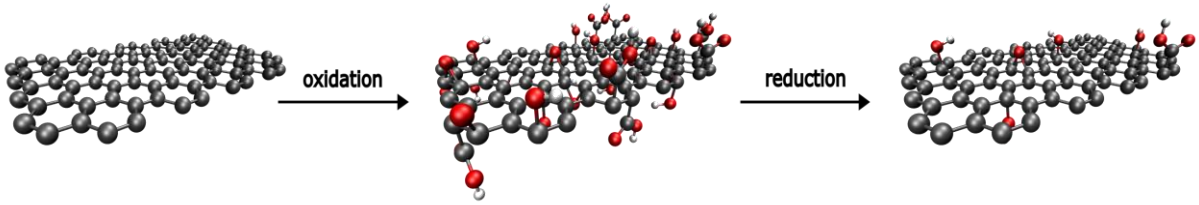

Figure 3: Scheme of structural changes of graphene after oxidation to GO followed by reduction to rGO.

GO exhibits significantly greater reactivity compared to graphite, a characteristic attributed to the presence of oxygen functional groups. These groups are amenable to typical organic reactions, paving the way for the further modification of GO. This capacity for modification is of paramount importance, as it facilitates the synthesis of functionalized graphene derivatives tailored for specific applications. The functionalization of GO has been the subject of extensive research over the years, resulting in the discovery and publication of numerous novel methodologies. A considerable portion of this literature focuses on the functionalization of GO with thiolated and aminated compounds, highlighting the breadth of potential modifications [28–30]. The development and application of functionalized GBM continue to advance across various research disciplines. These fields predominantly explore the utilization of graphene derivatives in drug delivery systems, biomedical sensors, antibacterial applications, and the removal of pollutants from water. The ongoing innovation in these areas underscores the versatile potential of GBM in addressing a wide array of scientific and environmental challenges [31–34].

A plethora of techniques is employed in the characterization of novel materials, encompassing microscopic methods such as Scanning Electron Microscopy (SEM) and Transmission Electron Microscopy (TEM), diffraction methods including X-Ray Diffraction (XRD) and Energy-Dispersive X-ray Spectroscopy (EDS), as well as the extensively utilized spectroscopic techniques: Fourier Transform Infrared Spectroscopy (FTIR) and Raman spectroscopy [35]. FTIR works by detecting the wavelengths at which a sample absorbs infrared radiation, creating a molecular fingerprint that is unique to its chemical composition. This method leverages the vibrations of the molecular bonds within a sample when exposed to IR radiation, providing insights into the molecular structure and functional groups present [36]. On the other hand, Raman spectroscopy involves illuminating a sample with a laser and analysing the scattered light. The frequency shift in this scattered light reveals vibrational modes in the molecules, allowing for the identification of chemical structures and the study of material properties [37]. The detailed understanding of quantum mechanisms underlying spectroscopic techniques has further enabled the modelling of these characterizations through quantum computations.

1.4 Quantum computations

Ab initio calculations, based on quantum mechanical principles, are used to solve the Schrödinger equation for electronic systems, primarily using the Hartree-Fock (HF) method.

This technique emerged from the need to simplify the many-body problem of electron interactions in a system, facilitated by the Born-Oppenheimer approximation, which separates the electronic motion from the nuclear motion. The HF method approximates the complex many-electron wavefunction as multiple one-electron wavefunctions, allowing for a tractable solution by assuming electrons move independently within an effective Coulombic field generated by other electrons and nuclei. The total energy calculation in HF includes the kinetic energy of electrons, nuclei-electron attractions and electron-electron repulsions [38]. However, HF does not account for electron correlation effects—interactions between electrons—which are significant for accurate energy calculations. This limitation is addressed in post-Hartree-Fock methods such as Configuration Interaction (CI), Multiconfiguration Self-Consistent Field (MCSCF), and Coupled Cluster (CC) techniques [39–41]. These methods enhance accuracy by better incorporating electron correlation, though they remain computationally intensive and are typically feasible only for smaller systems due to scaling issues.

Density Functional Theory (DFT) revolutionised the field of computational chemistry by offering an alternative approach to wavefunction-based methods like HF. DFT focuses on electron density rather than wave functions, simplifying the calculations, particularly for large systems. The foundation of DFT lies in the Hohenberg-Kohn theorems, which establish that the ground state properties of a system are uniquely determined by its electron density [42]. DFT translates the quantum behaviour of electrons into a three-dimensional problem, reducing the computational complexity significantly compared to traditional ab initio methods. The Kohn-Sham (KS) equations within DFT further refine the theory by introducing specific forms for the kinetic energy and exchange-correlation functionals, allowing for accurate calculations of electronic structures. These equations treat electrons in a fictitious non-interacting system to replicate the electron density of the real interacting system. The iterative KS scheme recalculates electron density until it converges to a desired level of precission [43]. Advancements in DFT include the development of various exchange-correlation functionals, from the Local Density Approximation (LDA) to more sophisticated ones like Generalized Gradient Approximation (GGA) and meta-GGA, which account for electron density gradients and kinetic energy density, respectively [44–46]. Hybrid functionals combine DFT methods with exact exchange from HF, offering improved accuracy for a wide range of chemical phenomena, though at a higher computational cost. Innovations continue with functionals designed for specific applications, ensuring DFT remains a pivotal tool in computational chemistry, capable of handling complex molecular systems efficiently and accurately.

Ab initio and DFT methods, which some literature also classifies ab initio, demand substantial computational resources for large systems, particularly with larger basis sets. Since the inception of computational chemistry, the limitations in computational capacity have prompted the development of semi-empirical methods. These methods reduce computational complexity through a series of approximations and the integration of empirical parameters, such as atomic ionization potentials and electron affinities, which are derived from experimental data or high-level theoretical calculations. Semi-empirical methods are beneficial for studying large organic molecules and complex reaction mechanisms where comprehensive ab initio approaches are computationally prohibitive. However, the dependence on empirical parameters means that their accuracy is confined to the compound types and specific conditions for which these parameters have been optimized. This often results in substantial discrepancies when these methods are applied to systems outside their validated range. In this study, we also employ the semi-empirical tight-binding method GFN2-xTB, developed by Grimme's group, which is instrumental for conducting simulations that are computationally intensive for standard ab initio and DFT methods [47].

Among computational methods, Density Functional Theory (DFT) stands out as the most effective in terms of precision and computational resource efficiency. The first introduction of DFT computational methods into popular Gaussian 3 software has markedly propelled the field of computational chemistry, witnessing a growing adoption among scientists [48]. Moreover, the availability of both paid and free software has provided access to these computational tools, allowing researchers to conduct these complex computations from their personal computers.

In this study, we have synthesized GBM employing both traditional (Hummers method) and novel (electrochemical method) fabrication techniques. Subsequently, these materials were functionalized with EDA to augment their chemical properties. For the first time, an exhaustive characterization of the resultant materials was undertaken to assess and compare the attributes of GBM synthesized *via* both methodologies. Furthermore, we engaged in computational modelling and performed calculations to elucidate the spectroscopic properties of these materials. In order to mitigate the computational demand typically associated with the analysis of extensive systems like graphene, simplified models and semi-empirical methods were employed. The findings from these computational analyses were then meticulously compared with experimental data, providing a comprehensive evaluation of the material characteristics and efficiency of these calculations.

2 Materials and Methods

2.1 Chemicals

Used chemicals were obtained as follows. Graphite powder was purchased from Merck (Prague, Czech Republic). Graphite foil 0.5 mm, 99.8% was purchased from ThermoScientific (Brno, Czech Republic). Ethylenediamine (EDA), potassium permanganate ($KMnO_4$), and hydrogen peroxide aqueous solution (H_2O_2, 30%) were purchased from Sigma-Aldrich (Prague, Czech Republic). Sodium persulfate ($Na_2S_2O_8$, 99%) and sulphuric acid (H_2SO_4, 98%) were purchased from Penta (Prague, Czech Republic).

2.2 Fabrication of the materials

In this study, we employed two distinct methodologies to synthesize oxidized GBM. The first, an older and conventional technique, is an improved version of the Hummers' method. This method utilizes graphite powder as the starting material and results in the production of graphite oxide (GrO), which could be exfoliated into graphene oxide through various methods, such as ultrasound treatment. The second, a more recent approach, is electrochemical exfoliation. This method uses solid graphite, typically in the form of a sheet or rod, as the precursor and yields graphene oxide (GO). Each method offers unique advantages in terms of yield, quality, and functional properties of the resulting GBM. The difference between graphene oxide and graphite oxide is just in the number of layers. In the literature, both materials are titled mostly GO. For the purpose of this work, GrO is referred to as material fabricated by Hummers method, and GO is material fabricated by electrochemical exfoliation.

2.2.1 Improved Hummers method

The procedure for the fabrication of graphite oxide (GrO) was conducted in accordance with protocols outlined in a work by Lavin-Lopez and colleagues [49]. Graphite powder, used as the precursor material, was not subjected to further purification. Initially, 5 g of graphite powder was introduced into a reaction vessel along with 250 mL of concentrated sulphuric acid. The mixture was stirred at room temperature for 24 hours. Following this initial mixing period, 30 g of potassium permanganate ($KMnO_4$), acting as a strong oxidising agent, was added. Subsequently, the reaction temperature was raised to 55 °C and the mixture was stirred continuously for 72 hours to promote oxidation. After this extended reaction period, 20 mL of 30% hydrogen peroxide was introduced into the mixture, leading to a colour change from dark brown to dark

yellow. This colour transition indicates the reduction of manganese from higher to lower oxidation states. The mixture was then allowed to settle, and the supernatant was decanted from the solid product. The resulting GrO was subjected to multiple washing and separation cycles using distilled water in a centrifuge until a neutral pH was reached. Finally, the clean GrO was frozen and subsequently dried *via* lyophilisation to obtain the final product. A schematic of the reaction steps is depicted in Figure 4 .

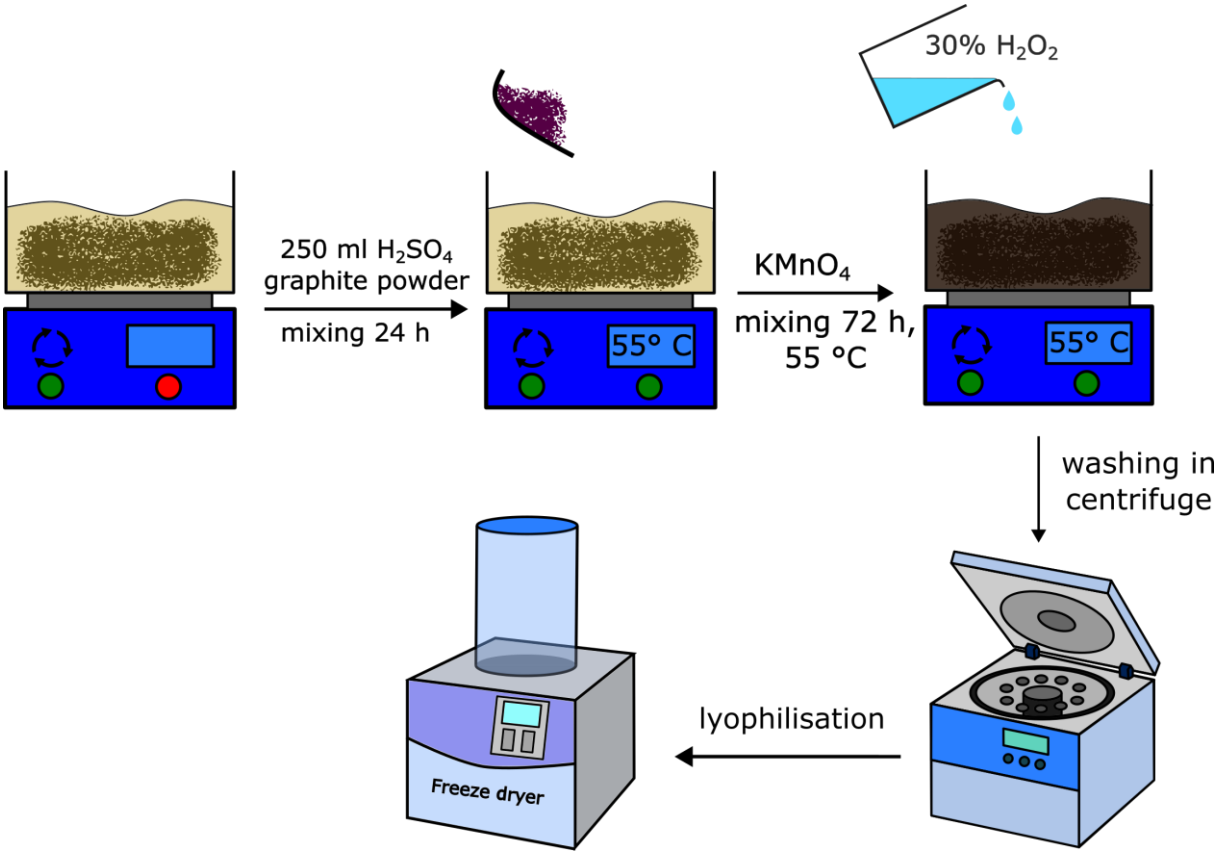

Figure 4: Individual steps of GrO fabrication through modified Hummers method.

2.2.2 Electrochemical exfoliation

Electrochemical exfoliation represents a distinct approach from traditional methods for synthesizing graphene oxide (GO), as it avoids the use of hazardous chemicals such as concentrated acids and strong oxidizing agents. Instead, this method utilizes an applied electrostatic potential along with various electrolytes, which not only facilitate the exfoliation process but also act as an oxidizing agent [50]. The electrochemical exfoliation process can be delineated into two sequential steps. Initially, the applied electric field induces the dissociation of water molecules, generating hydroxyl groups with a negative charge. These hydroxyl groups are then

attracted to the anode, where they slightly oxidize the edges of the graphite sheets. This initial oxidation allows electrolyte molecules, which are also dissociated by the electric field, to intercalate between the graphite layers. The intercalated ions from the electrolyte subsequently undergo electrochemical reactions with the graphite. These reactions lead to the oxidation of graphite and the concomitant release of gas molecules, such as O_2 and others, depending on the electrolyte, which usually is sulphate-based; thus, often SO_2 is released. The expansion of these gas molecules generates sufficient force to overcome the van der Waals forces between the graphite layers, thereby facilitating the exfoliation of graphite into GO [19].

In this study, a 0.1 M solution of sodium persulfate ($Na_2S_2O_8$) was employed as the electrolyte for the electrochemical exfoliation process. Upon application of an electric field, the $Na_2S_2O_8$ decomposes into sulphate radicals, which facilitate the electrochemical oxidation of graphite. Previous studies have demonstrated the efficacy of sulphates in the electrochemical production of graphene oxide (GO), making them a preferred choice for this application [51]. Contrary to the horizontal configurations commonly reported in the literature, our experimental setup featured a vertical arrangement [52]. The cathode, composed of titanium mesh, was positioned at the bottom of the reactor, while the anode, a graphite sheet, was suspended approximately 2 cm above the centre of the cathode. In order to maintain a consistent spacing of 2 cm, the graphite sheet was gradually lowered as the reaction progressed. Both electrodes were connected to a direct current (DC) power supply, with an electric potential set at 10 volts. Upon activation of the DC power, the immediate release of gases (a combination of O_2 and SO_2) was observed, alongside the initial exfoliation of GO. A schematic of the entire setup and reaction steps is depicted in Figure 5. The reaction continued with the progressive lowering of the graphite sheet until complete exfoliation of the entire volume of graphite sheet was achieved. Subsequently, the mixture containing the electrolyte and produced GO was subjected to vacuum filtration. During filtration, the product was thoroughly washed with distilled water to remove any residual electrolyte, ensuring a neutral pH. The purified GO was then frozen and dried *via* lyophilisation. All steps of this procedure are depicted in Figure 5 and mechanism of electrochemical exfoliation is illustrated in Figure 6.

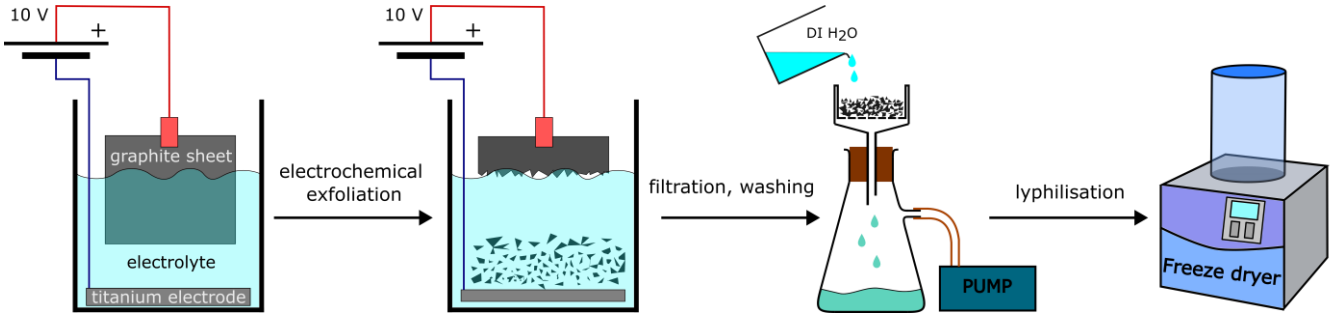

Figure 5: Scheme illustrating process of fabricating graphene oxide by electrochemical exfoliation.

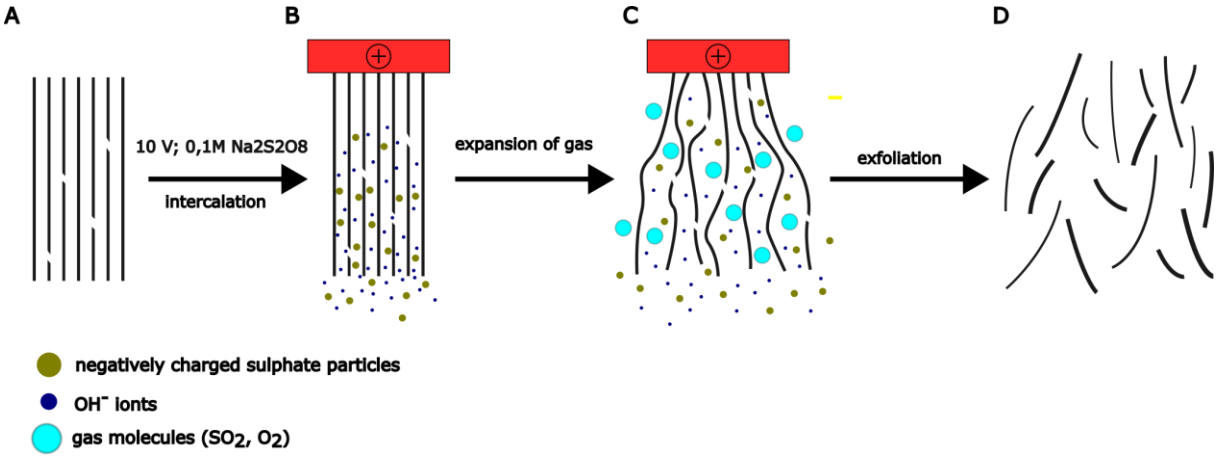

Figure 6: Mechanism of electrochemical exfoliation, where **A** is bulk sheet of graphite with its layers, **B** is intercalation of negatively charged particles between planes of graphite, **C** production of gas molecules as a result of electrochemical reaction and **D** single or few layers thick exfoliated graphene sheets.

2.2.3 Functionalization of GO and GrO by EDA

The functionalization process for the oxidized GBM, specifically GO and GrO, was uniformly executed. Initially, a 4 g/L aqueous dispersion of GO and GrO was prepared *via* ultrasonic treatment for 20 minutes. These dispersions were then transferred to sealable reactors, which were subsequently placed in an oil bath maintained at a temperature of 70 °C. Upon the dispersions reaching 70 °C, ethylenediamine (EDA) was introduced at a volumetric ratio of 4 µL per mL of dispersion [53]. The reaction proceeded within these sealed reactors for a duration of 3 hours under constant mixing at a speed of 300 rpm. Post-reaction, the products were

subjected to a washing process using a 1:1 mixture of water and ethanol, facilitated by centrifugation. The washed products were then frozen and subsequently lyophilized to yield a dry powder of functionalized GO-EDA and GrO-EDA.

2.3 Characterization

All fabricated materials were comprehensively characterised by FTIR (Nicolet iZ10, Thermo Scientific, USA) and Raman spectroscopy (Raman microscope DXR. Thermo scientific, USA). FTIR spectra were measured in the range from 4000 to 400 cm^{-1} with a resolution of 4 cm^{-1}. Raman spectra were measured in the range from 3500 to 50 cm^{-1} by a 532 nm excitation laser. SEM analysis was carried out by Helios 5 PFIB CXe (Thermo Scientific, USA) and EDS analysis was done by Ulti Max EDS detector (Oxford Instruments, UK). All characterization procedures were carried out with materials after fabrication (as described previously) in solid (powder) form without further purification.

2.3.1 FTIR

FTIR, an essential analytical technique for characterizing materials by measuring their infrared absorption or emission spectra, was used to characterize fabricated materials. In FTIR spectroscopy, an infrared light is passed through a sample, and the absorbance or transmittance of light at different wavelengths is recorded, generating a spectrum. This spectrum represents the molecular fingerprint of the sample, with unique peaks corresponding to the vibrations of the bonds within the molecules [54]. This method is particularly useful in identifying functional groups and understanding the molecular structures of GBM like graphene oxide and functionalized graphene oxide. For graphene oxide, FTIR can detect oxygen-containing functional groups such as hydroxyl, epoxy, and carbonyl. When graphene oxide is functionalized, FTIR helps confirm the attachment of new functional groups, such as amine groups, indicating successful functionalization, which is crucial for tailoring material properties for specific applications [55].

2.3.2 Raman spectroscopy

Raman spectroscopy stands out as an indispensable tool for characterizing GBM, particularly emphasizing the D and G bands owing to their intrinsic significance. The D band, associated with disorder-induced phonon modes, reflects structural imperfections and defects within the graphene lattice, offering insights into its quality and purity. The G band in Raman

spectroscopy indicates that graphene has a well-ordered crystal structure and a network of carbon atoms bonded in an sp^2 configuration. The ratio of these bands, often denoted as the I_D/I_G ratio, is one of the most important metrics for evaluating structural disorder and graphene layer stacking [56]. However, from Raman spectroscopy studies of a single layer of graphene with precisely tailored defects, we know about the existence of other bands, which are not noticeably visible at first glance and often have to be found through deconvolution of original spectra, which serve as a better tool to understanding properties of GBM [57]. The most significant is the understanding that the apparent G peak (G_{app}), commonly labelled as G peak, around 1600 cm^{-1} is a superposition of real G and D´ peaks [58]. Understanding these two peaks and their contribution to visible G_{app} was mainly studied in the transition from GO to rGO [59]. Raman spectroscopy not only enables non-destructive and rapid characterization but also provides intricate details regarding the structural properties and quality of GBM.

2.4 Computational methods

In this research, the quantum chemistry package ORCA 5.0.4 was utilized to conduct an in-depth study of the spectroscopic properties of GBM [60]. The inherently periodic structure of graphene and graphite, characterized by occasional defects such as holes, presents significant challenges in accurately modelling these systems. Moreover, the structure of functionalized GBM can vary considerably depending on the synthesis method employed. Although both the modified Hummers method and the electrochemical method used in this study effectively oxidize graphite powder, the resultant GO may differ in terms of structural defects, the degree of oxidation, and the distribution of oxygen-containing functional groups on the GO surface. Furthermore, the increase in the number of atoms in the system corresponds to an exponential increase in the system's degrees of freedom, necessitating a corresponding rise in computational resources for the calculations.

Given these complexities, we opted to use coronene as a simplified model to investigate the behaviour of GBM. Various studies have validated this approach as an effective method for modelling GBM [61–63]. Employing coronene as a model significantly reduces the computational costs, thereby allowing for the use of more precise functionals and higher basis sets that would otherwise be computationally prohibitive.

2.4.1 Modelling of a system

In this study, all models were constructed using Avogadro, an open-source molecular editor [64]. Initial coordinates for coronene were sourced from Avogadro's built-in library. Subsequently, functionalized models of coronene were derived from the base structure. In order to facilitate the quick and efficient preselection of conformers with the lowest energy for each system, a simple Python script leveraging the RDKit library was employed [65]. This script generated several random conformers, which were then swiftly optimized using Avogadro's built-in optimization tools. The conformer with the lowest energy was selected as the input for further calculations.

In order to comprehensively study the spectroscopic properties of GBM, multiple models were created using coronene as a simplified model. Specifically, 6 models of coronene were designed to investigate the structure of graphene oxide (GO). One model represented pure coronene without any functionalization, while the other three models were oxygenated derivatives, each incorporating one of the primary oxygen functional groups found on the surface of GO. A similar approach was applied to model functionalized GO-EDA. For this derivative, two models were created, each representing the structure following the reaction of EDA with one of the individual oxygen functional groups. All models used for our calculations, with their optimized geometries, are depicted in Figure 7.

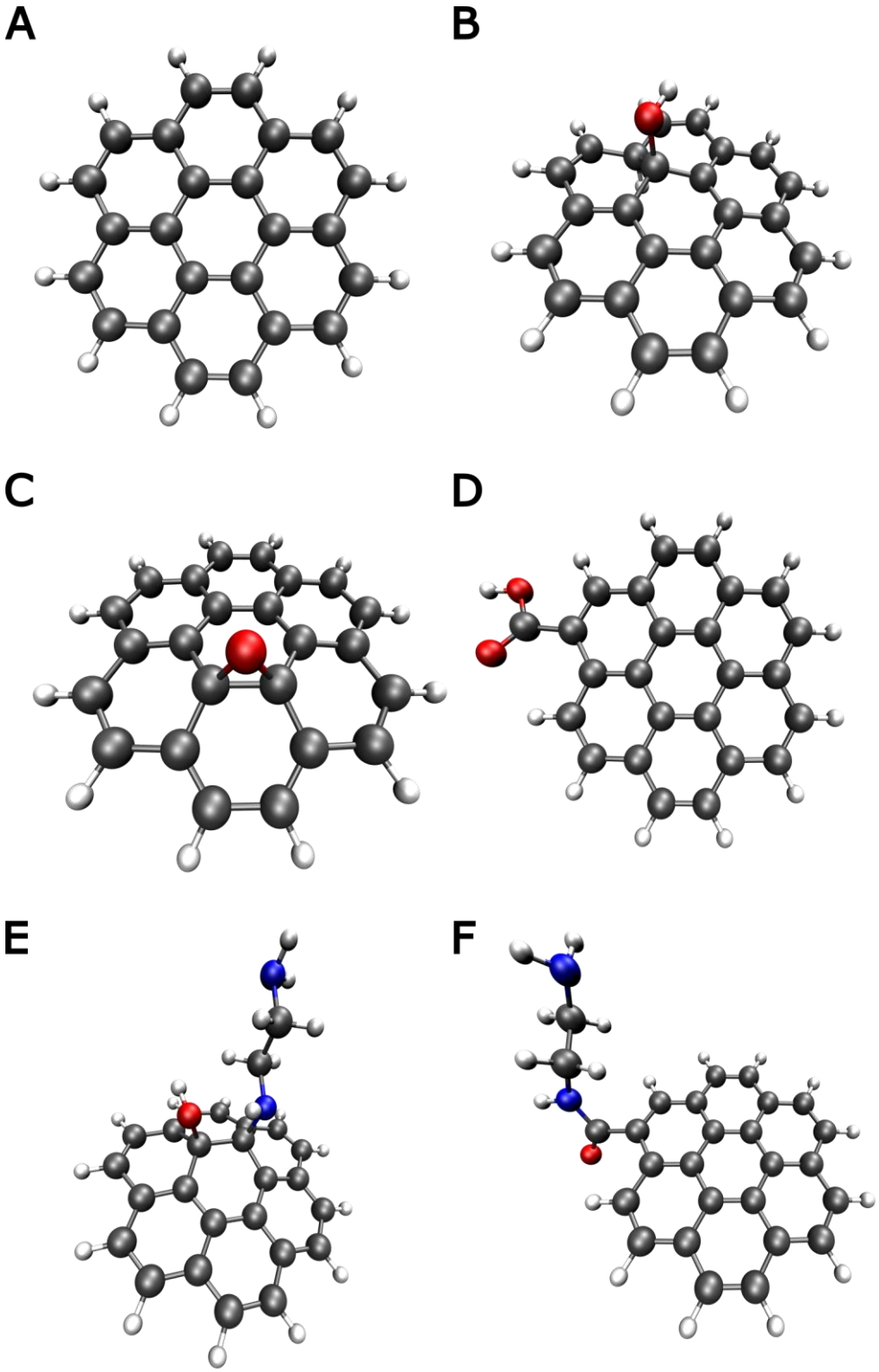

Figure 7: Models of coronene with different functional groups. **A** coronene, **B** coronene-hydroxyl group, **C** coronene-epoxy group, **D** coronene-carboxyl group, **E** coronene-epoxy group after reaction with EDA, **F** coronene-carboxyl group after reaction with EDA.

2.4.2 Details of computations

Calculations were conducted using the ORCA 5.0.4 software, employing DFT and semi-empirical methods. Predominantly, literature on DFT calculations for GBM has utilized the hybrid B3LYP functional [66]. However, given the continual advancements in the theory of DFT functionals and the introduction of new computational methods by researchers, we also incorporated the newer composite functional r2SCAN-3c based on the comprehensive review by Bursch et al. [47, 67]. Alongside these DFT functionals, the semi-empirical method GFN2-xTB was employed for its significant computational speed advantage—approximately two to three orders of magnitude faster—to assess its efficacy in calculating the spectroscopic properties of our simplified system of GBM [68].

All calculations were carried out on the def2-TZVPP basis set [69]. In order to ensure a fair comparison of their performance in spectroscopic applications, all models were optimized using the r2SCAN-3c method. The optimized structures then served as the input for further calculations (with all mentioned methods) to determine the spectroscopic properties, specifically the Infrared (IR) and Raman spectra. Calculations of vibrational frequencies were done for each model separately. The resulting spectroscopic data were combined to appropriately model functional groups of a given material (except for clear coronene as a model of graphite) using Multiwfn, allowing for a comprehensive evaluation of each method's effectiveness [70].

3 Results and discussion

3.1 SEM and EDS analysis

The morphology of fabricated materials was characterized using SEM images (Figure 8). The material produced by the Hummers method (GrO) exhibited a denser structure with smaller and less distinct individual sheets. In contrast, the material prepared through electrochemical exfoliation (GO) displayed a less condensed structure featuring larger individual sheets. Both results are in accordance with published literature [71, 72]. The functionalization by EDA, apart from the small deformation of the sheets, did not affect the structure of the materials.

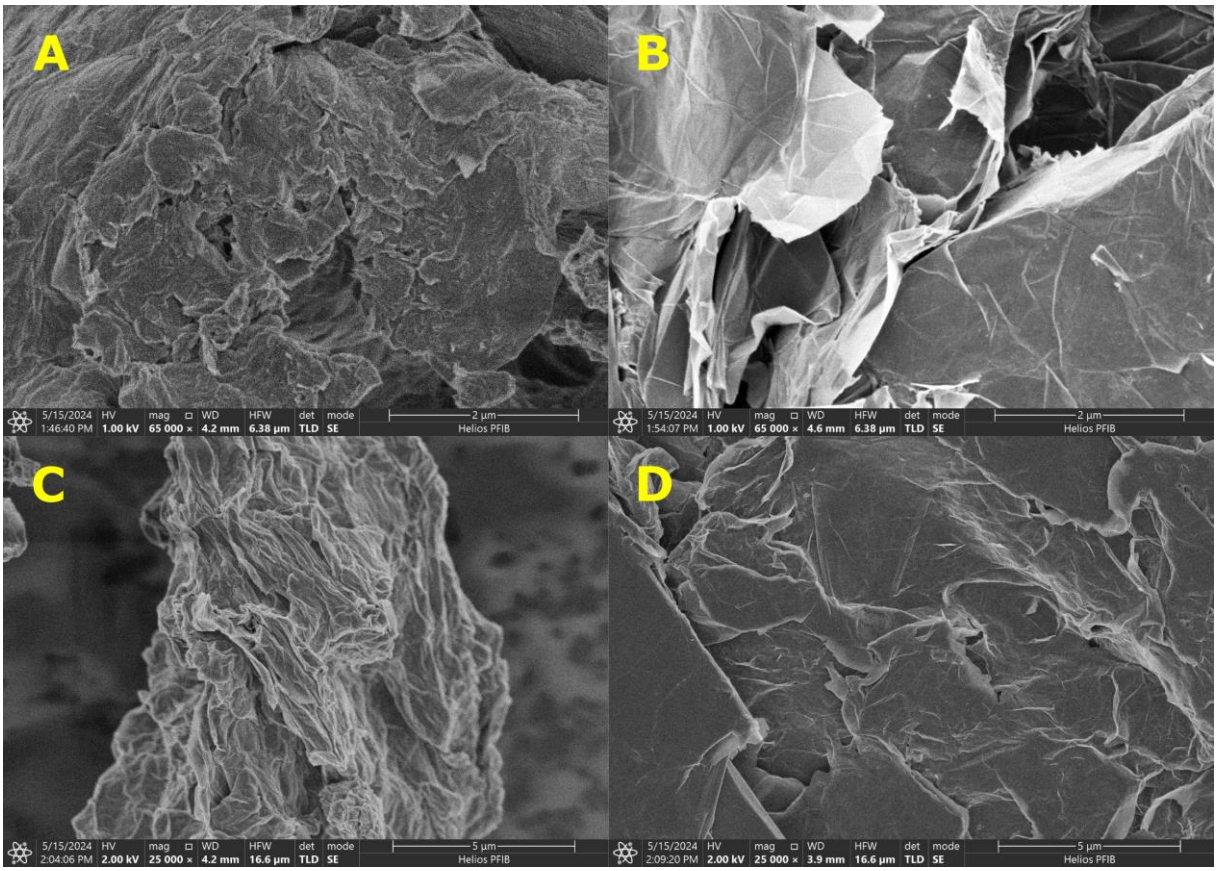

Figure 8: SEM images of **A** GrO, **B** GO, **C** GrO-EDA and **D** GO-EDA.

The elemental composition of all synthetized materials was obtained by EDS analysis. The sample of GrO was found to contain a higher proportion of oxygen atoms, approximately 33 at%, in contrast to GO, which contained about 15 at% of oxygen. It should be mentioned that the EDS cannot provide a precise comparison in such heterogeneous samples due to the fact that it is a point analysis. Nonetheless, in both samples, small traces of sulphur, likely impurities from fabrication methods, were found. Following the reaction with EDA, nitrogen was

detected in both materials, confirming successful functionalization. Specifically, in GrO-EDA, oxygen and nitrogen were measured at approximately 23 at% and 6 at%, respectively. In GO-EDA the levels were approximately 5 at% for oxygen and 9 at% for nitrogen. Despite the lower oxygen content in materials prepared by electrochemical exfoliation, they are more susceptible to functionalization by EDA. This may indicate that GO has more reactive oxygen functional groups, such as epoxy functionality, on its surface.

3.2 Raman spectra

The spectroscopic analysis yielded spectra for both fabrication methods *via* Raman spectroscopy that are consistent with findings reported in the existing literature [73]. For all examined materials, the D and G_{app} bands were distinctly observed at approximately 1350 cm^{-1} and 1600 cm^{-1}, respectively. In addition to the D and G_{app} bands, other characteristic bands such as 2D, D+G, and 2D′ were also detected across all spectra, albeit at varying intensities. These bands observed at frequencies around 2700 cm^{-1}, 2930 cm^{-1}, and 3200 cm^{-1}, respectively, are typical for GBM exhibiting certain defect levels and align with documented literature findings [74]. The spectra corresponding to each fabrication method are depicted in Figure 9. In addition, the spectra of graphite—identical in both plots—exhibit a D+D′′ peak. A slight presence of the D′ peak is also observable in the graphite spectra, which has been emphasized by fitting a yellow line to the data, as detailed in Section 2.3.2. Probably, these peaks are not visible in other spectra due to the samples being analysed in their solid (powder) state as fabricated, without undergoing further purification or separation into individual sheets of graphite.

The positions of the D and G_{app} bands remain nearly constant across both oxidation methods and even after functionalization with EDA. A comparison with the graphite spectra confirms that the position of the D band is stable, maintaining the same frequency. As anticipated, the relative intensity of the D peak compared to the G peak increased following oxidation; this enhancement was slightly amplified by subsequent functionalization by EDA. The relative intensification of the D peak was more pronounced in samples prepared through electrochemical exfoliation. In comparison to graphite, the G_{app} peak exhibited a slight shift towards higher frequencies, suggesting an increased contribution from the D′ peak. The functionalization process introduced a significant shoulder between the D and G_{app} peaks, relative to graphite. This shoulder has been previously identified as the D′′ band, associated with the presence of amorphous carbon. In the sample designated as GrO (fabricated by modified Hummers

method), this shoulder appears more prominent, indicating a higher content of amorphous carbon, which we attribute to the use of strong chemicals during the fabrication process. For bands at higher frequencies (such as 2D, D+G, and 2D′) around 2900 cm^{-1}, the relative intensity is greater in materials fabricated through electrochemical exfoliation. Notably, in the GrO-EDA samples, the peaks at 2D and 2D′ were nearly undetectable.

In order to elucidate the structural properties of our GBM, we calculated the I_D/I_G ratios for all materials [75]. Intensities were calculated directly from the spectra, the deconvolution of the spectra into separate peaks was not considered in this study. For graphite, the I_D/I_G ratio stands at 0.13. This value, as expected, is the lowest when compared with modified materials and reveals some structural imperfections in natural graphite powder. Typically, in pure graphite—a fully periodic system of sp^2-bonded carbon atoms—no D peak should be observed, as it arises from defects within the sp^2 plane. In natural graphite, we assume that the majority of the defects contributing to the slight presence of the D peak are holes within the individual planes, as no chemical modification is expected. For oxidized GBM fabricated using the modified Hummer′s method and electrochemical exfoliation, the calculated I_D/I_G ratios are 0.94 and 0.95, respectively, aligning with findings reported in the literature [76, 77]. These results suggest that the defects induced by the oxidation process, which now encompass not only structural holes but also the successful incorporation of oxygen functional groups onto the carbon atoms, are comparable in both materials, apart from the previously discussed higher content of amorphous carbon in GrO. For materials functionalized with EDA, the I_D/I_G ratios are 1.00 and 1.10 for GrO-EDA and GO-EDA, respectively. These ratios exceed those observed for GrO and GO, indicating that functionalization was successfully achieved. Based on these values, it can be assumed that the structure of GO-EDA was more significantly impacted than that of GrO-EDA, resulting in a higher degree of functionalization.

Based on the research by A. K. King and colleagues, a comparative analysis of the oxygen content in our materials was conducted using the obtained Raman spectra [59]. According to their findings, the difference in frequencies between the D′ and G bands can be correlated with the C/O ratio of graphene oxides, where a smaller difference indicates a lower C/O ratio. Although the D′ peak is not visible in our spectra, it can be obtained simply by halving the vibration of the 2D′ peak. For our materials, the calculated differences in the D′ − G band frequencies are 1.3 for GO and 2.7 for GrO, respectively. Without the application of additional methods to determine a more precise C/O ratio, we can only make a comparative assumption that the oxygen content in the fabricated materials is relatively similar. Nonetheless, GO, which

was prepared by electrochemical exfoliation, based on these data, might have achieved a slightly higher level of oxidation. This comparative approach underscores the utility of Raman spectroscopy in gauging the oxidation levels in graphene oxides, reflecting subtle variations in their chemical compositions.

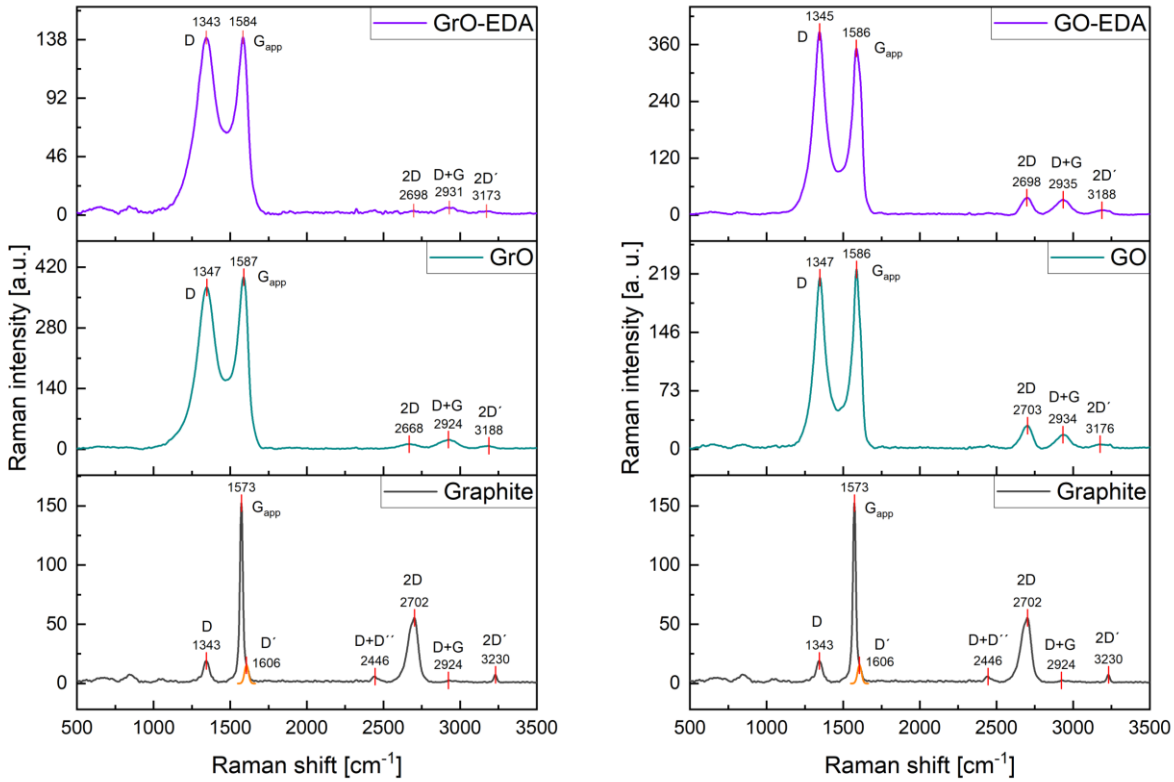

Figure 9: Raman spectra of graphite (same for both) as a precursor and of fabricated materials, on the left by modified Hummer´s method and on the right by electrochemical exfoliation.

3.3 FTIR spectra

Analogous to the Raman spectroscopy approach, FTIR spectra were obtained for all four fabricated materials, as well as for graphite, which was used as the precursor material. As anticipated, the FTIR spectra of graphite did not exhibit any significant peaks. Notably, while some studies have identified minor bands corresponding to adsorbed water moieties and vibrations of C=C at approximately 3300 cm^{-1} and 1600 cm^{-1}, respectively, this feature was not observed in our analyses [78, 79]. This further underscores the chemical resistivity of bulk graphite [80]. All spectra are depicted in Figure 10.

The FTIR spectra of GrO display a broad band spanning from approximately 3700 cm^{-1} to 2500 cm^{-1}, with its peak intensity at 3217 cm^{-1}. This characteristic broad band arises from the collective single-bond stretching vibrations of O-H and C-H bonds [81]. The peak observed at 1722 cm^{-1} is attributed to the C=O stretching vibrations of carboxyl and possibly carbonyl groups [82]. Subsequent to this, the band at 1599 cm^{-1} is indicative of C=C vibrations within the sp^2 carbon network [83]. The spectral region extending from approximately 1300 cm^{-1} to 950 cm^{-1} is associated with C-O or O-H vibrations stemming from various oxygen functional groups. Within this range, the peak at 1034 cm^{-1}, which exhibits the highest intensity, is identified as the C-O vibrations of tertiary hydroxyl groups on the surface of the graphene [84]. Additionally, a slight shoulder detectable at 1150 cm^{-1} can be assigned to C-O stretching vibrations of epoxy groups [83].

The functionalization of GrO with EDA results in the emergence of a small peak at 3337 cm^{-1} within the FTIR spectrum, attributable to N-H stretching vibrations [85]. This peak adds intensity to the broad band comprising O-H and C-H vibrations. A comparative analysis of GrO-EDA and GrO reveals the complete disappearance of the peak associated with C=O vibrations of carboxylic acid, suggesting that most carboxyl groups reacted with EDA. The peak at 1593 cm^{-1}, indicative of C=C vibrations, remains unchanged. Additionally, a marginal decrease in spectral intensity is observed in the region from approximately 1300 cm^{-1} to 950 cm^{-1}, which in GrO corresponded to C-O or O-H vibrations from various oxygen functionalities. The peak assigned to C-O vibrations of the hydroxyl group is slightly shifted post-functionalization from 1034 cm^{-1} to 1053 cm^{-1}, yet remains evident. A general decrease in oxygen functionalities, resulting from reactions with EDA, unveils a new peak at 1346 cm^{-1}, which can be assigned to O-H vibrations of hydroxyl groups [84]. These findings suggest that the majority of hydroxyl groups remained unaffected by the functionalization process. The successful functionalization of GrO by EDA is primarily confirmed by the appearance of a new peak at 1232 cm^{-1}, corresponding to vibrations of newly formed C-N bonds, alongside the disappearance of vibrations from carboxyl and epoxy groups [86].

The FTIR spectra of GO and GO-EDA do not exhibit the same quality as those of GrO and its GrO-EDA, likely due to variations in structural properties resulting from different fabrication methods. Nonetheless, they share similar characteristic peaks. Similar to GrO, a broad band from approximately 3400 cm^{-1} to 2800 cm^{-1} is detected in GO, which is attributed to the combined vibrations of C-H and O-H. Additionally, a small peak at 1704 cm^{-1} is observed, which is associated with C=O vibrations of the carboxylic group, and a peak at 1637 cm^{-1} is indicative of C=C stretching. The bands at 1394 cm^{-1} and 1061 cm^{-1} are likely related to the O-H and C-O stretching vibrations of hydroxyl groups, respectively.

In the case of GO-EDA, a noticeable change is observed in the broad band at higher frequencies, indicating the addition of N-H vibrations with a peak at 3323 cm^{-1}. This alteration suggests the incorporation of amine groups into the structure. Moreover, the band associated with O-H vibrations has shifted toward lower frequencies, moving from 1394 cm^{-1} to 1336 cm^{-1}, which may be attributed to the influence of newly formed C-N bonds. Additionally, an intense new peak at 823 cm^{-1} has emerged, representing the vibrations of new C-N bonds, further confirming the successful functionalization of the material with EDA [87].

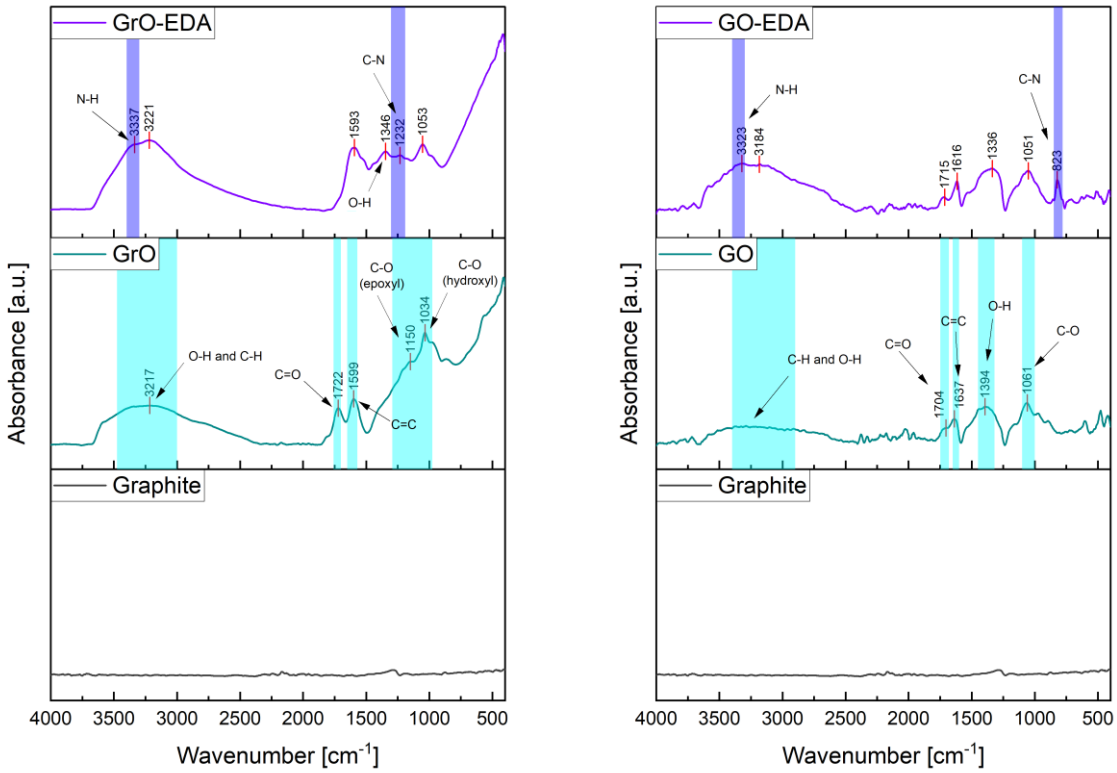

Figure 10: FTIR spectra of graphite and fabricated materials, on the left by modified Hummer´s method and on the right by electrochemical exfoliation.

3.4 Comparison with computations

We have computed the vibrational frequencies for both Raman and infrared (IR) spectra using the methods described earlier. The graphite spectra were calculated exclusively from the coronene model. For the oxidized GBM, the spectra were generated through a combination of individual calculations from models of coronene and coronene with various oxygen functional groups. Spectra of materials functionalized by EDA were obtained by combining the calculated spectra from models of coronene, coronene with a hydroxyl group (which is not expected to react with EDA), and coronene modified with epoxy and carboxyl groups post-reaction with EDA. These calculated spectra are then compared with selected spectra obtained from experimental analysis of GO and GO-EDA.

The calculated Raman frequencies are illustrated in Figure 11. The frequencies obtained *via* both DFT methods (B3LYP and r2SCAN-3c) show a minimal discrepancy, with differences within 50 cm^{-1}. These methods predict that the D band of graphite appears at frequencies approximately 20 cm^{-1} and 40 cm^{-1} higher than the experimental value when calculated by B3LYP and r2SCAN-3c, respectively. For the G band, both DFT methods compute frequencies that are about 80 cm^{-1} higher than the observed values. This trend of overestimating the frequencies for the D and G bands is also evident in other models. While the DFT methods seem to predict the position of the 2D' band accurately, the intensity is significantly overestimated due to the numerous C-H bonds on the edges of coronene. Additionally, the DFT calculations suggest the presence of the D+G band, which is consistently misplaced by approximately 30 cm^{-1}. This consistent overestimation across the spectra indicates a potential systematic error in the theoretical approach employed for these specific bands.

DFT methods, apart from omitting the 2D band, seem to predict the Raman spectra of graphene-based material quite precisely and could be used to approximate experimental spectra. On the contrary, the semi-empirical method of these simplified models delivers inaccurate results.

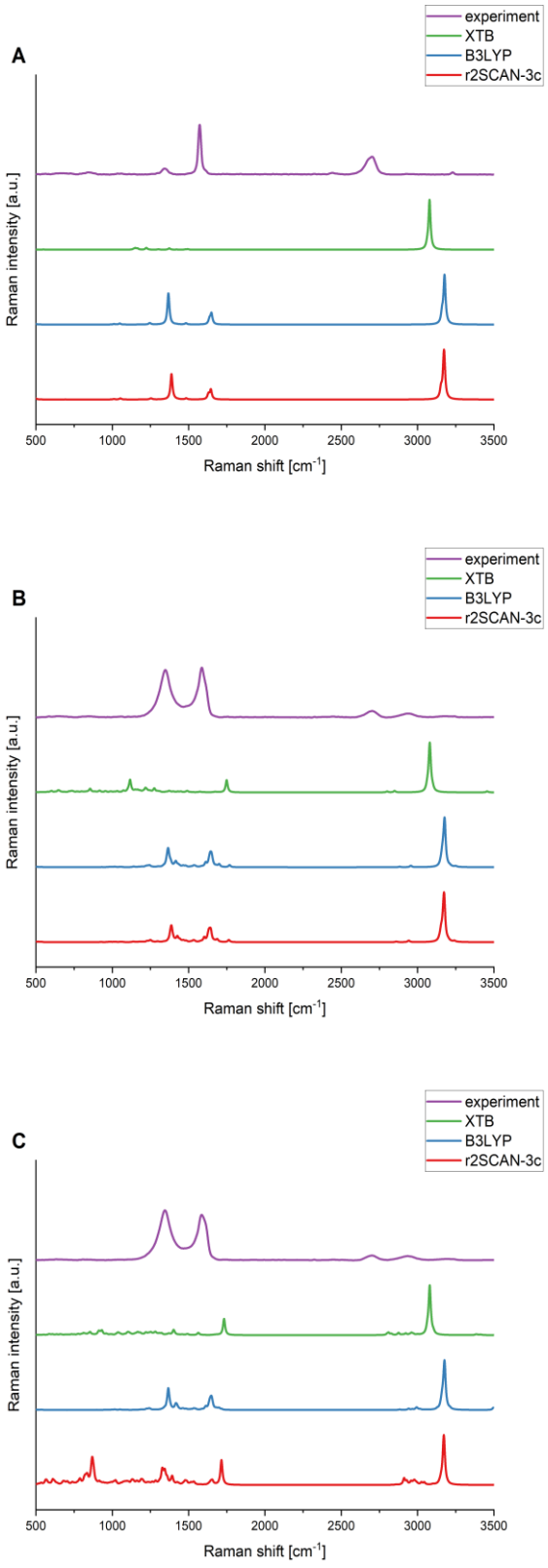

Figure 11: Calculated Raman spectra of **A** graphite, **B** GO, **C** GO-EDA by coronene and functionalized-coronene models in comparison with obtained experimental data. Presented spectra were calculated by two DFT methods (B3LYP and r^2SCAN-3c) and semi-empirical method GFN2-xTB (in short XTB).

The calculations of the IR spectra are presented in Figure 12. Spectra of graphite are omitted as no peaks were measured in the experimental spectra. Overall, the calculated spectra by DFT methods appear to predict some functional groups' positions accurately. The maximum position of the peak responsible for C-H vibrations is off by only about 50 cm^{-1} across the entire broad peak. Additionally, the vibrations of the –COOH and –OH, expected at approximately 1760 cm^{-1} and 1340 cm^{-1}, seem to be correctly predicted, diverging only about 40 cm^{-1} from the experimental value. In contrast to calculations of Raman spectra, the performance of the semi-empirical method for calculations of IR spectra does not differ as drastically from DFT, apart from relative intensities, because semi-empirical methods are built for calculations on larger systems. Therefore, the semi-empirical method could be used for quick aproximatory predictions.

In computations, vibrational frequencies are calculated for the ground state, which is typically represented as an isolated molecule in a gas phase, which, together with approximations to harmonic vibrations, may present a certain level of inaccuracies. The chosen computational methods, with a simplification of the complex system to the models of coronene, have demonstrated their capability, within a certain level of accuracy, to predict the vibrational frequencies of specific functionalities of GBM. Although it seems that different strategies need to be employed to model such a complex system with many interactions as a whole, While the semi-empirical GFN2-xTB method did not perform as well compared to the DFT methods, the differences are not substantial. We also have to consider the significantly lower computational demand of the semi-empirical method for computational resources, being able to complete calculations (on a standard PC) in minutes, whereas DFT might take over a day. Semi-empirical methods are our best option for modelling a larger system. Such a system would more closely resemble the real structure of GBM, suggesting that GFN2-xTB could offer significant advantages in accurately modeling these complex structures.

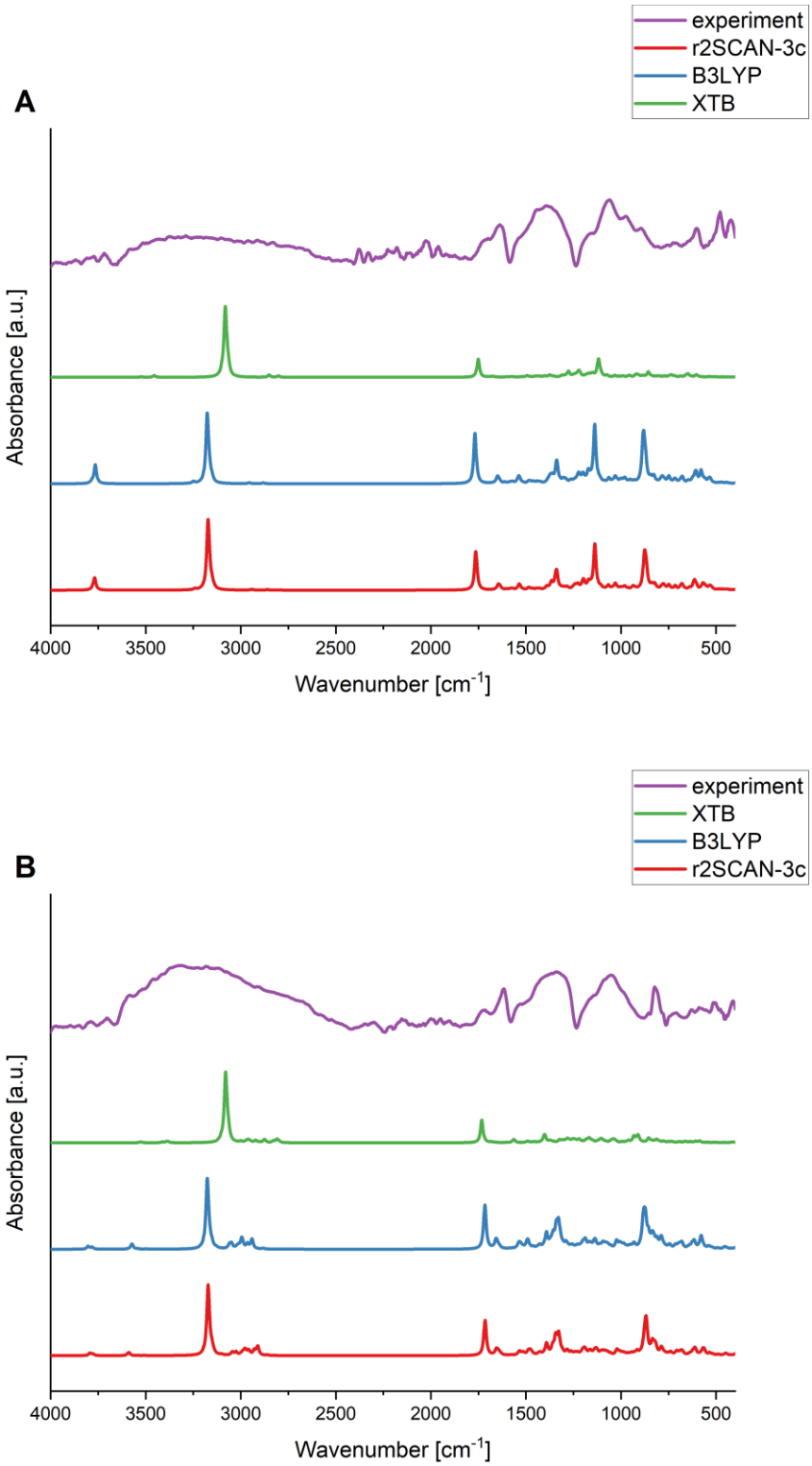

Figure 12: Calculated IR spectra of **A** GO, **B** GO-EDA by coronene and functionalized-coronene models in comparison with obtained experimental data. Presented spectra were calculated by two DFT methods (B3LYP and r^2SCAN-3c) and semi-empirical method GFN2-xTB (in short XTB).

Conclusion

In this study, we successfully fabricated oxidized GBM using two distinct methodologies: a common method involving hazardous chemicals and a novel, environmentally friendly procedure.

The traditional approach utilized an improved Hummers method with slight modifications, employing strong oxidizing agents and acids over a prolonged period. In contrast, the innovative method of electrochemical exfoliation employed electric potential and an electrolyte, presenting a more environmentally friendly alternative for the fabrication of GBM. Subsequently, these materials were functionalized using EDA. All synthesized materials underwent comprehensive characterization through SEM, EDS as well as FTIR and Raman spectroscopy, confirming their successful preparation. Raman spectroscopy analysis, based on the I_D/I_G ratio, suggested comparable levels of defects in materials fabricated by both methods. However, a larger portion of amorphous carbon was inferred in the material produced by the modified Hummers method, indicated by the distinct shoulder between the D and G peaks. The I_D/I_G ratios also suggested that the structure of materials fabricated by electrochemical exfoliation was more significantly altered by EDA functionalization. FTIR results confirmed the successful oxidation of the GBM for both methods, as evidenced by the appearance of bands primarily associated with carboxyl, epoxy, and hydroxyl functional groups. Additionally, FTIR analysis indicated successful functionalization by EDA. Results from spectroscopic methods were further confirmed by EDS analysis, which showed a larger content of oxygen in material prepared by the Hummers method and a larger amount of nitrogen atoms in EDA functionalized material prepared by electrochemical exfoliation, supporting the result from Raman spectroscopy.

We further compared these spectroscopic characterization results (Raman and FTIR) with outcomes from DFT and semi-empirical computational methods. Our attempt to model the spectroscopic properties of GBM using a simplified coronene model delivered sufficient, but not completely precise, results for the approximate modelling of Raman spectra by DFT methods, while the semi-empirical method has proven to be insufficient for the calculation of Raman spectra by this simplified strategy. Calculated IR spectra, by the described methods, are able to quite precisely predict the vibrational frequencies of specific functionalities, although, for spectral calculations of such a complex system, it seems that a different approach needs to be employed. For the calculations of IR spectra, the difference in performance between DFT and the semi-empirical method was not that noticeable despite saving a large amount of computational resources. This suggests that it would be advisable to calculate IR spectra on a larger system,

representing GBM, with the semi-empirical method, and for Raman, it seems inevitable to use DFT methods with a lower basis set to reduce computational cost.

References

[1] LIU, Yuan; Yu HUANG and Xiangfeng DUAN. Van der Waals integration before and beyond two-dimensional materials. online. *Nature*, vol. 567 (2019), no. 7748, pp. 323–333. Available from: https://doi.org/10.1038/s41586-019-1013-x.

[2] Nanochemistry. online. In: Anonymous. *Supramolecular Chemistry*, pp. 899–939. John Wiley & Sons, Ltd, 2009. Available from: https://doi.org/10.1002/9780470740880.ch15.

[3] SMALLEY, Richard E. Discovering the fullerenes. online. *Reviews of Modern Physics*, vol. 69 (1997), no. 3, pp. 723–730. Available from: https://doi.org/10.1103/RevModPhys.69.723.

[4] IIJIMA, Sumio. Helical microtubules of graphitic carbon. online. *Nature*, vol. 354 (1991), no. 6348, pp. 56–58. Available from: https://doi.org/10.1038/354056a0.

[5] NOVOSELOV, K. S.; A. K. GEIM; S. V. MOROZOV; D. JIANG; Y. ZHANG et al. Electric Field Effect in Atomically Thin Carbon Films. online. *Science*, vol. 306 (2004), no. 5696, pp. 666–669. Available from: https://doi.org/10.1126/science.1102896.

[6] Classification of Nanomaterials. online. In: Anonymous. *Nanomaterials in Advanced Medicine*, pp. 47–62. John Wiley & Sons, Ltd, 2019. Available from: https://doi.org/10.1002/9783527818921.ch3.

[7] GEIM, A. K. Graphene: Status and Prospects. online. *Science*, vol. 324 (2009), no. 5934, pp. 1530–1534. Available from: https://doi.org/10.1126/science.1158877.

[8] HOSSEINGHOLIPOURASL, Ali; Sharifah HAFIZAH SYED ARIFFIN; Yasser D. AL-OTAIBI; Elnaz AKBARI; Fatimah KH HAMID et al. Analytical Approach to Study Sensing Properties of Graphene Based Gas Sensor. online. *Sensors*, vol. 20 (2020), no. 5, p. 1506. Available from: https://doi.org/10.3390/s20051506.

[9] GUPTA, Banshi D.; Anisha PATHAK and Vivek SEMWAL. Carbon-Based Nanomaterials for Plasmonic Sensors: A Review. online. *Sensors*, vol. 19 (2019), no. 16, p. 3536. Available from: https://doi.org/10.3390/s19163536.

[10] ERSAN, Gamze; Onur G. APUL; Francois PERREAULT and Tanju KARANFIL. Adsorption of organic contaminants by graphene nanosheets: A review. online. *Water Research*, vol. 126 (2017), pp. 385–398. Available from: https://doi.org/10.1016/j.watres.2017.08.010.

[11] YANG, Ying-Kui; Cuiping HAN; Beibei JIANG; James IOCOZZIA; Chengen HE et al. Graphene-based materials with tailored nanostructures for energy conversion and storage. online. *Materials Science and Engineering: R: Reports*, vol. 102 (2016), pp. 1–72. Available from: https://doi.org/10.1016/j.mser.2015.12.003.

[12] AFROJ, Shaila; Sirui TAN; Amr M. ABDELKADER; Kostya S. NOVOSELOV and Nazmul KARIM. Highly Conductive, Scalable, and Machine Washable Graphene-Based E-Textiles for Multifunctional Wearable Electronic Applications. online. *Advanced Functional Materials*, vol. 30 (2020), no. 23, p. 2000293. Available from: https://doi.org/10.1002/adfm.202000293.

[13] HUANG, Liang; Diana SANTIAGO; Patricia LOYSELLE and Liming DAI. Graphene-Based Nanomaterials for Flexible and Wearable Supercapacitors. online. *Small*, vol. 14 (2018), no. 43, p. 1800879. Available from: https://doi.org/10.1002/smll.201800879.

[14] LIN, Li; Hailin PENG and Zhongfan LIU. Synthesis challenges for graphene industry. online. *Nature Materials*, vol. 18 (2019), no. 6, pp. 520–524. Available from: https://doi.org/10.1038/s41563-019-0341-4.

[15] DONG, Lei; Zhongxin CHEN; Xiaoxu ZHAO; Jianhua MA; Shan LIN et al. A non-dispersion strategy for large-scale production of ultra-high concentration graphene slurries in water. online. *Nature Communications*, vol. 9 (2018), no. 1, p. 76. Available from: https://doi.org/10.1038/s41467-017-02580-3.

[16] WHITENER, Keith E.; Woo K. LEE; Paul M. CAMPBELL; Jeremy T. ROBINSON and Paul E. SHEEHAN. Chemical hydrogenation of single-layer graphene enables completely reversible removal of electrical conductivity. online. *Carbon*, vol. 72 (2014), pp. 348–353. Available from: https://doi.org/10.1016/j.carbon.2014.02.022.

[17] HUMMERS, William S. Jr. and Richard E. OFFEMAN. Preparation of Graphitic Oxide. online. *Journal of the American Chemical Society*, vol. 80 (1958), no. 6, pp. 1339–1339. Available from: https://doi.org/10.1021/ja01539a017.

[18] MARCANO, Daniela C.; Dmitry V. KOSYNKIN; Jacob M. BERLIN; Alexander SINITSKII; Zhengzong SUN et al. Improved Synthesis of Graphene Oxide. online. *ACS Nano*, vol. 4 (2010), no. 8, pp. 4806–4814. Available from: https://doi.org/10.1021/nn1006368.

[19] PARVEZ, Khaled; Zhong-Shuai WU; Rongjin LI; Xianjie LIU; Robert GRAF et al. Exfoliation of Graphite into Graphene in Aqueous Solutions of Inorganic Salts. online. *Journal of the American Chemical Society*, vol. 136 (2014), no. 16, pp. 6083–6091. Available from: https://doi.org/10.1021/ja5017156.

[20] SU, Ching-Yuan; Ang-Yu LU; Yanping XU; Fu-Rong CHEN; Andrei N. KHLOBYSTOV et al. High-Quality Thin Graphene Films from Fast Electrochemical Exfoliation. online. *ACS Nano*, vol. 5 (2011), no. 3, pp. 2332–2339. Available from: https://doi.org/10.1021/nn200025p.

[21] WU, Weiming; Changsong ZHANG and Shaogang HOU. Electrochemical exfoliation of graphene and graphene-analogous 2D nanosheets. online. *Journal of Materials Science*, vol. 52 (2017), no. 18, pp. 10649–10660. Available from: https://doi.org/10.1007/s10853-017-1289-x.

[22] PEI, Songfeng; Qinwei WEI; Kun HUANG; Hui-Ming CHENG and Wencai REN. Green synthesis of graphene oxide by seconds timescale water electrolytic oxidation. online. *Nature Communications*, vol. 9 (2018), no. 1, p. 145. Available from: https://doi.org/10.1038/s41467-017-02479-z.

[23] YAN, Jia-An and M. Y. CHOU. Oxidation functional groups on graphene: Structural and electronic properties. online. *Physical Review B*, vol. 82 (2010), no. 12, p. 125403. Available from: https://doi.org/10.1103/PhysRevB.82.125403.

[24] GANDHI, Muniyappan Rajiv; Subramanyan VASUDEVAN; Atsushi SHIBAYAMA and Manabu YAMADA. Graphene and Graphene-Based Composites: A Rising Star in Water Purification - A Comprehensive Overview. online. *ChemistrySelect*, vol. 1 (2016), no. 15, pp. 4358–4385. Available from: https://doi.org/10.1002/slct.201600693.

[25] PEI, Songfeng and Hui-Ming CHENG. The reduction of graphene oxide. online. *Carbon*, vol. 50 (2012), no. 9, pp. 3210–3228. Available from: https://doi.org/10.1016/j.carbon.2011.11.010.

[26] RAO, Sanjeev; Jahnavee UPADHYAY; Kyriaki POLYCHRONOPOULOU; Rehan UMER and Raj DAS. Reduced Graphene Oxide: Effect of Reduction on Electrical Conductivity. online. *Journal of Composites Science*, vol. 2 (2018), no. 2, p. 25. Available from: https://doi.org/10.3390/jcs2020025.

[27] MURARU, Sebastian; Jorge S. BURNS and Mariana IONITA. GOPY: A tool for building 2D graphene-based computational models. online. *SoftwareX*, vol. 12 (2020). Available from: https://doi.org/10.1016/j.softx.2020.100586.

[28] HE, Hongkun and Chao GAO. General Approach to Individually Dispersed, Highly Soluble, and Conductive Graphene Nanosheets Functionalized by Nitrene Chemistry. online. *Chemistry of Materials*, vol. 22 (2010), no. 17, pp. 5054–5064. Available from: https://doi.org/10.1021/cm101634k.

[29] LAI, Linfei; Luwei CHEN; Da ZHAN; Li SUN; Jinping LIU et al. One-step synthesis of NH2-graphene from in situ graphene-oxide reduction and its improved electrochemical properties. online. *Carbon*, vol. 49 (2011), no. 10, pp. 3250–3257. Available from: https://doi.org/10.1016/j.carbon.2011.03.051.

[30] DIAGBOYA, Paul N.; Herry K. MMAKO; Ezekiel D. DIKIO and Fanyana M. MTUNZI. Synthesis of amine and thiol dual functionalized graphene oxide for aqueous sequestration of lead. online. *Journal of Environmental Chemical Engineering*, vol. 7 (2019), no. 6, p. 103461. Available from: https://doi.org/10.1016/j.jece.2019.103461.

[31] LUO, Yanan; Xiaoli CAI; He LI; Yuehe LIN and Dan DU. Hyaluronic Acid-Modified Multifunctional Q-Graphene for Targeted Killing of Drug-Resistant Lung Cancer Cells. online. *ACS applied materials & interfaces*, vol. 8 (2016), no. 6, pp. 4048–4055. Available from: https://doi.org/10.1021/acsami.5b11471.

[32] NAEEM, Hina; Muhammad AJMAL; Raheela QURESHI; Sedra MUNTHA and Muhammad FAROOQ. Facile synthesis of graphene oxide-silver nanocomposite for decontamination of water from multiple pollutants by adsorption, catalysis and antibacterial activity. online. *Journal of environmental management*, vol. 230 (2018), pp. 199–211. Available from: https://doi.org/10.1016/j.jenvman.2018.09.061.

[33] MAITI, Debabrata; Xiangmin TONG; Xiaozhou MOU and Kai YANG. Carbon-Based Nanomaterials for Biomedical Applications: A Recent Study. online. *Frontiers in Pharmacology*, vol. 9 (2019). Available from: https://doi.org/10.3389/fphar.2018.01401.

[34] TAJIK, Somayeh; Zahra DOURANDISH; Kaiqiang ZHANG; Hadi BEITOLLAHI; Quyet Van LE et al. Carbon and graphene quantum dots: a review on syntheses, characterization, biological and sensing applications for neurotransmitter determination. online. *RSC ADVANCES*, vol. 10 (2020), no. 26, pp. 15406–15429. Available from: https://doi.org/10.1039/d0ra00799d. Web of Science ID: WOS:000530037900045.

[35] HU, Maocong; Zhenhua YAO; Xianqin WANG; Maocong HU; Zhenhua YAO et al. Characterization techniques for graphene-based materials in catalysis. online. *AIMS Materials Science*, vol. 4 (2017), no. 3, pp. 755–788. Available from: https://doi.org/10.3934/matersci.2017.3.755. Cc_license_type: cc_by-Primary_atype: AIMS Materials ScienceSubject_term: ReviewSubject_term_id: Review.

[36] NANDIYANTO, Asep Bayu Dani; Risti RAGADHITA and Meli FIANDINI. Interpretation of Fourier Transform Infrared Spectra (FTIR): A Practical Approach in the Polymer/Plastic Thermal Decomposition. online. *Indonesian Journal of Science and Technology*, vol. 8 (2023), no. 1, pp. 113–126. Available from: https://doi.org/10.17509/ijost.v8i1.53297.

[37] FERRARI, Andrea C. and Denis M. BASKO. Raman spectroscopy as a versatile tool for studying the properties of graphene. online. *Nature Nanotechnology*, vol. 8 (2013), no. 4, pp. 235–246. Available from: https://doi.org/10.1038/nnano.2013.46.

[38] CHUVYLKIN, N. D. and E. A. SMOLENSKII. Quantum chemistry of many-electron systems: high-priority aspects. online. *Russian Chemical Bulletin*, vol. 64 (2015), no. 10, pp. 2277–2283. Available from: https://doi.org/10.1007/s11172-015-1154-5.

[39] DAVID SHERRILL, C. and Henry F. SCHAEFER. The Configuration Interaction Method: Advances in Highly Correlated Approaches. online. In: LÖWDIN, Per-Olov; John R. SABIN; Michael C. ZERNER and Erkki BRÄNDAS (ed.). *Advances in Quantum Chemistry*, pp. 143–269. Academic Press, 1999. Available from: https://doi.org/10.1016/S0065-3276(08)60532-8.

[40] SCHMIDT, Michael W. and Mark S. GORDON. THE CONSTRUCTION AND INTERPRETATION OF MCSCF WAVEFUNCTIONS. online. *Annual Review of Physical Chemistry*, vol. 49 (1998), no. Volume 49, 1998, pp. 233–266. Available from: https://doi.org/10.1146/annurev.physchem.49.1.233.

[41] KÜMMEL, Hermann. Origins of the Coupled Cluster Method. online. *Theoretica chimica acta*, vol. 80 (1991), no. 2, pp. 81–89. Available from: https://doi.org/10.1007/BF01119615.

[42] HOHENBERG, P. and W. KOHN. Inhomogeneous Electron Gas. online. *Physical Review*, vol. 136 (1964), no. 3B, pp. B864–B871. Available from: https://doi.org/10.1103/PhysRev.136.B864.

[43] KOHN, W. and L. J. SHAM. Self-Consistent Equations Including Exchange and Correlation Effects. online. *Physical Review*, vol. 140 (1965), no. 4A, pp. A1133–A1138. Available from: https://doi.org/10.1103/PhysRev.140.A1133.

[44] SAHNI, Viraht; K. -P. BOHNEN and Manoj K. HARBOLA. Analysis of the local-density approximation of density-functional theory. online. *Physical Review A*, vol. 37 (1988), no. 6, pp. 1895–1907. Available from: https://doi.org/10.1103/PhysRevA.37.1895.

[45] PERDEW, John P.; Kieron BURKE and Matthias ERNZERHOF. Generalized Gradient Approximation Made Simple. online. *Physical Review Letters*, vol. 77 (1996), no. 18, pp. 3865–3868. Available from: https://doi.org/10.1103/PhysRevLett.77.3865.

[46] PERDEW, John P.; Jianmin TAO; Viktor N. STAROVEROV and Gustavo E. SCUSERIA. Meta-generalized gradient approximation: Explanation of a realistic nonempirical density functional. online. *The Journal of Chemical Physics*, vol. 120 (2004), no. 15, pp. 6898–6911. Available from: https://doi.org/10.1063/1.1665298.

[47] GRIMME, Stefan; Andreas HANSEN; Sebastian EHLERT and Jan-Michael MEWES. r2SCAN-3c: A "Swiss army knife" composite electronic-structure method. online. *The Journal of Chemical Physics*, vol. 154 (2021), no. 6. Available from: https://doi.org/10.1063/5.0040021.

[48] JONES, R. O. Density functional theory: Its origins, rise to prominence, and future. online. *Reviews of Modern Physics*, vol. 87 (2015), no. 3, pp. 897–923. Available from: https://doi.org/10.1103/RevModPhys.87.897.

[49] LAVIN-LOPEZ, Maria del Prado; Amaya ROMERO; Jesus GARRIDO; Luz SANCHEZ-SILVA and José Luis VALVERDE. Influence of Different Improved Hummers Method Modifications on the Characteristics of Graphite Oxide in Order to Make a More Easily Scalable Method. online. *Industrial & Engineering Chemistry Research*, vol. 55 (2016), no. 50, pp. 12836–12847. Available from: https://doi.org/10.1021/acs.iecr.6b03533.

[50] LIU, Fei; Chaojun WANG; Xiao SUI; Muhammad Adil RIAZ; Meiying XU et al. Synthesis of graphene materials by electrochemical exfoliation: Recent progress and future potential. online. *Carbon Energy*, vol. 1 (2019), no. 2, pp. 173–199. Available from: https://doi.org/10.1002/cey2.14.

[51] PARK, Si-Woo; Byungkwon JANG; Han KIM; Jimin LEE; Ji Young PARK et al. Highly Water-Dispersible Graphene Nanosheets From Electrochemical Exfoliation of Graphite. online. *Frontiers in Chemistry*, vol. 9 (2021). Available from: https://doi.org/10.3389/fchem.2021.699231.

[52] PARVEZ, Khaled; Rongjin LI; Sreenivasa Reddy PUNIREDD; Yenny HERNANDEZ; Felix HINKEL et al. Electrochemically Exfoliated Graphene as Solution-Processable, Highly Conductive Electrodes for Organic Electronics. online. *ACS Nano*, vol. 7 (2013), no. 4, pp. 3598–3606. Available from: https://doi.org/10.1021/nn400576v.

[53] JANG, Jaewon; Insu PARK; Sang-Soo CHEE; Jun-Ho SONG; Yesol KANG et al. Graphene oxide nanocomposite membrane cooperatively cross-linked by monomer and polymer overcoming the trade-off between flux and rejection in forward osmosis. online. *Journal of Membrane Science*, vol. 598 (2020), p. 117684. Available from: https://doi.org/10.1016/j.memsci.2019.117684.

[54] GRIFFITHS, Peter R. and James A. De HASETH. *Fourier Transform Infrared Spectrometry*. John Wiley & Sons, 2007. ISBN 978-0-470-10629-7. Google-Books-ID: C_c0GVe8MX0C.

[55] DEHGHANZAD, Behzad; Mir Karim Razavi AGHJEH; Omid RAFEIE; Akram TAVAKOLI and Amin Jameie OSKOOIE. Synthesis and characterization of graphene and functionalized graphene via chemical and thermal treatment methods. online. *RSC Advances*, vol. 6 (2016), no. 5, pp. 3578–3585. Available from: https://doi.org/10.1039/C5RA19954A.

[56] ZÓLYOMI, V.; J. KOLTAI and J. KÜRTI. Resonance Raman spectroscopy of graphite and graphene. online. *physica status solidi (b)*, vol. 248 (2011), no. 11, pp. 2435–2444. Available from: https://doi.org/10.1002/pssb.201100295.

[57] LÓPEZ-DÍAZ, David; Marta LÓPEZ HOLGADO; José L. GARCÍA-FIERRO and M. Mercedes VELÁZQUEZ. Evolution of the Raman Spectrum with the Chemical Composition of Graphene Oxide. online. *The Journal of Physical Chemistry C*, vol. 121 (2017), no. 37, pp. 20489–20497. Available from: https://doi.org/10.1021/acs.jpcc.7b06236.

[58] LUO, Zhiqiang; Chunxiao CONG; Jun ZHANG; Qihua XIONG and Ting YU. The origin of sub-bands in the Raman D-band of graphene. online. *Carbon*, vol. 50 (2012), no. 11, pp. 4252–4258. Available from: https://doi.org/10.1016/j.carbon.2012.05.008.

[59] KING, Alice A. K.; Benjamin R. DAVIES; Nikan NOORBEHESHT; Peter NEWMAN; Tamara L. CHURCH et al. A New Raman Metric for the Characterisation of Graphene oxide and its Derivatives. online. *Scientific Reports*, vol. 6 (2016), no. 1, p. 19491. Available from: https://doi.org/10.1038/srep19491.

[60] NEESE, Frank. Software update: The ORCA program system—Version 5.0. online. *WIREs Computational Molecular Science*, vol. 12 (2022), no. 5, p. e1606. Available from: https://doi.org/10.1002/wcms.1606.

[61] WILSON, Jake; Noelia FAGINAS-LAGO; Jelle VEKEMAN; Inmaculada G. CUESTA; José SÁNCHEZ-MARÍN et al. Modeling the Interaction of Carbon Monoxide with Flexible Graphene: From Coupled Cluster Calculations to Molecular-Dynamics Simulations. online. *ChemPhysChem*, vol. 19 (2018), no. 6, pp. 774–783. Available from: https://doi.org/10.1002/cphc.201701387.

[62] SAHA, Bapan and Pradip Kr. BHATTACHARYYA. Anion···π interaction in oxoanion-graphene complex using coronene as model system: A DFT study. online. *Computational and Theoretical Chemistry*, vol. 1147 (2019), pp. 62–71. Available from: https://doi.org/10.1016/j.comptc.2018.12.005.

[63] ROHINI, K.; Daniel M. R. SYLVINSON and R. S. SWATHI. Intercalation of HF, H2O, and NH3 Clusters within the Bilayers of Graphene and Graphene Oxide: Predictions from Coronene-Based Model Systems. online. *The Journal of Physical Chemistry A*, vol. 119 (2015), no. 44, pp. 10935–10945. Available from: https://doi.org/10.1021/acs.jpca.5b05702.

[64] HANWELL, Marcus D.; Donald E. CURTIS; David C. LONIE; Tim VANDERMEERSCH; Eva ZUREK et al. Avogadro: an advanced semantic chemical editor, visualization, and analysis platform. online. *Journal of Cheminformatics*, vol. 4 (2012), no. 1, p. 17. Available from: https://doi.org/10.1186/1758-2946-4-17.

[65] LANDRUM, Greg; Paolo TOSCO; Brian KELLEY; Ricardo RODRIGUEZ; David COSGROVE et al. *rdkit/rdkit: 2024_03_1 (Q1 2024) Release*. Program. Release_2024_03_2. Zenodo, 2024. Available from: https://doi.org/10.5281/zenodo.11102446.

[66] STEPHENS, P. J.; F. J. DEVLIN; C. F. CHABALOWSKI and M. J. FRISCH. Ab Initio Calculation of Vibrational Absorption and Circular Dichroism Spectra Using Density Functional Force Fields. online. *The Journal of Physical Chemistry*, vol. 98 (1994), no. 45, pp. 11623–11627. Available from: https://doi.org/10.1021/j100096a001.

[67] BURSCH, Markus; Jan-Michael MEWES; Andreas HANSEN and Stefan GRIMME. Best-Practice DFT Protocols for Basic Molecular Computational Chemistry**. online. *Angewandte Chemie*, vol. 134 (2022), no. 42, p. e202205735. Available from: https://doi.org/10.1002/ange.202205735.

[68] BANNWARTH, Christoph; Sebastian EHLERT and Stefan GRIMME. GFN2-xTB—An Accurate and Broadly Parametrized Self-Consistent Tight-Binding Quantum Chemical Method with Multipole Electrostatics and Density-Dependent Dispersion Contributions. online. *Journal of Chemical Theory and Computation*, vol. 15 (2019), no. 3, pp. 1652–1671. Available from: https://doi.org/10.1021/acs.jctc.8b01176.

[69] WEIGEND, Florian and Reinhart AHLRICHS. Balanced basis sets of split valence, triple zeta valence and quadruple zeta valence quality for H to Rn: Design and assessment of accuracy. online. *Physical Chemistry Chemical Physics*, vol. 7 (2005), no. 18, pp. 3297–3305. Available from: https://doi.org/10.1039/B508541A.

[70] LU, Tian and Feiwu CHEN. Multiwfn: A multifunctional wavefunction analyzer. online. *Journal of Computational Chemistry*, vol. 33 (2012), no. 5, pp. 580–592. Available from: https://doi.org/10.1002/jcc.22885.

[71] CHEN, Chun-Hu; Shin HU; Jyun-Fu SHIH; Chang-Ying YANG; Yun-Wen LUO et al. Effective Synthesis of Highly Oxidized Graphene Oxide That Enables Wafer-scale Nanopatterning: Preformed Acidic Oxidizing Medium Approach. online. *Scientific Reports*, vol. 7 (2017), no. 1, p. 3908. Available from: https://doi.org/10.1038/s41598-017-04139-0.

[72] GEE, Chuen-Ming; Chien-Chih TSENG; Feng-Yu WU; Hsin-Ping CHANG; Lain-Jong LI et al. Flexible transparent electrodes made of electrochemically exfoliated graphene sheets from low-cost graphite pieces. online. *Displays*, vol. 34 (2013), no. 4, pp. 315–319. Available from: https://doi.org/10.1016/j.displa.2012.11.002.

[73] HAFIZ, Syed Muhammad; Richard RITIKOS; Thomas James WHITCHER; Nadia Md RAZIB; Daniel Chia Sheng BIEN et al. A practical carbon dioxide gas sensor using room-temperature hydrogen plasma reduced graphene oxide. online. *SENSORS AND ACTUATORS B-CHEMICAL*, vol. 193 (2014), pp. 692–700. Available from: https://doi.org/10.1016/j.snb.2013.12.017. Web of Science ID: WOS:000330113600096.

[74] MA, Bing; Raul D. RODRIGUEZ; Alexey RUBAN; Sergey PAVLOV and Evgeniya SHEREMET. The correlation between electrical conductivity and second-order Raman modes of laser-reduced graphene oxide. online. *Physical Chemistry Chemical Physics*, vol. 21 (2019), no. 19, pp. 10125–10134. Available from: https://doi.org/10.1039/C9CP00093C.

[75] EIGLER, Siegfried; Christoph DOTZER and Andreas HIRSCH. Visualization of defect densities in reduced graphene oxide. online. *Carbon*, vol. 50 (2012), no. 10, pp. 3666–3673. Available from: https://doi.org/10.1016/j.carbon.2012.03.039.

[76] KIM, Seon-Guk; Ok-Kyung PARK; Joong Hee LEE and Bon-Cheol KU. Layer-by-layer assembled graphene oxide films and barrier properties of thermally reduced graphene oxide membranes. online. *Carbon letters*, vol. 14 (2013), no. 4, pp. 247–250. Available from: https://doi.org/10.5714/CL.2013.14.4.247.

[77] SENGUPTA, Iman; Suddhapalli S. S. Sharat KUMAR; Surjya K. PAL and Sudipto CHAKRABORTY. Characterization of structural transformation of graphene oxide to reduced graphene oxide during thermal annealing. online. *Journal of Materials Research*, vol. 35 (2020), no. 9, pp. 1197–1204. Available from: https://doi.org/10.1557/jmr.2020.55.

[78] KUMARA, Gamaralalage R. A.; Herath Mudiyanselage G. T. A. PITAWALA; Buddika KARUNARATHNE; Mantilaka Mudiyanselage M. G. P. G. MANTILAKA; Rajapakse Mudiyanselage G. RAJAPAKSE et al. Development of a chemical-free floatation technology for the purification of vein graphite and characterization of the products. online. *Scientific Reports*, vol. 11 (2021), no. 1, p. 22713. Available from: https://doi.org/10.1038/s41598-021-02101-9.

[79] HADI, Alireza; Jafar ZAHIRIFAR; Javad KARIMI-SABET and Abolfazl DASTBAZ. Graphene nanosheets preparation using magnetic nanoparticle assisted liquid phase exfoliation of graphite: The coupled effect of ultrasound and wedging nanoparticles. online. *ULTRASONICS SONOCHEMISTRY*, vol. 44 (2018), pp. 204–214. Available from: https://doi.org/10.1016/j.ultsonch.2018.02.028. Web of Science ID: WOS:000433265300023.

[80] CHANG, Dong Wook; Eun Kwang LEE; Eun Yeob PARK; Hojeong YU; Hyun-Jung CHOI et al. Nitrogen-Doped Graphene Nanoplatelets from Simple Solution Edge-Functionalization for n-Type Field-Effect Transistors. online. *Journal of the American Chemical Society*, vol. 135 (2013), no. 24, pp. 8981–8988. Available from: https://doi.org/10.1021/ja402555n.

[81] CHEN, Da; Hongbin FENG and Jinghong LI. Graphene Oxide: Preparation, Functionalization, and Electrochemical Applications. online. *Chemical Reviews*, vol. 112 (2012), no. 11, pp. 6027–6053. Available from: https://doi.org/10.1021/cr300115g.

[82] HE, Dongning; Zheng PENG; Wei GONG; Yongyue LUO; Pengfei ZHAO et al. Mechanism of a green graphene oxide reduction with reusable potassium carbonate. online. *RSC Advances*, vol. 5 (2015), no. 16, pp. 11966–11972. Available from: https://doi.org/10.1039/C4RA14511A.

[83] BAGRI, Akbar; Cecilia MATTEVI; Muge ACIK; Yves J. CHABAL; Manish CHHOWALLA et al. Structural evolution during the reduction of chemically derived graphene oxide. online. *Nature Chemistry*, vol. 2 (2010), no. 7, pp. 581–587. Available from: https://doi.org/10.1038/nchem.686.

[84] MERMOUX, M; Y CHABRE and A ROUSSEAU. FTIR and 13C NMR study of graphite oxide. online. *Carbon*, vol. 29 (1991), no. 3, pp. 469–474. Available from: https://doi.org/10.1016/0008-6223(91)90216-6.

[85] DA SILVA, Cleiser T. P.; Johny P. MONTEIRO; Eduardo RADOVANOVIC and Emerson M. GIROTTO. Unprecedented high plasmonic sensitivity of substrates based on gold nanoparticles. online. *Sensors and Actuators B: Chemical*, vol. 191 (2014), pp. 152–157. Available from: https://doi.org/10.1016/j.snb.2013.09.109.

[86] ZHOU, Fanglei; Ngoc Tien HUYNH; Qiaobei DONG; Weiwei L. XU; Huazheng LI et al. Ultrathin, ethylenediamine-functionalized graphene oxide membranes on hollow fibers for CO_2 capture. online. *JOURNAL OF MEMBRANE SCIENCE*, vol. 573 (2019), pp. 184–191. Available from: https://doi.org/10.1016/j.memsci.2018.11.080. Web of Science ID: WOS:000454830600020.

[87] WAN, Wubo; Lingli LI; Zongbin ZHAO; Han HU; Xiaojuan HAO et al. Ultrafast Fabrication of Covalently Cross-linked Multifunctional Graphene Oxide Monoliths. online. *Advanced Functional Materials*, vol. 24 (2014), no. 31, pp. 4915–4921. Available from: https://doi.org/10.1002/adfm.201303815.